

# Dark Radiation with Baryon Acoustic Oscillations from DESI 2024<sup>0</sup> and the $H_0$ tension<sup>0</sup>

Itamar J. Allali,<sup>1,\*</sup> Alessio Notari,<sup>2,3,†</sup> and Fabrizio Rompineve<sup>4,5,‡</sup>

<sup>1</sup>*Department of Physics, Brown University, Providence, RI 02912, USA*<sup>1</sup>

<sup>2</sup>*Departament de Física Quàntica i Astrofísica & Institut de Ciències del Cosmos (ICCUB),*<sup>2</sup>

*Universitat de Barcelona, Martí i Franquès 1, 08028 Barcelona, Spain.*<sup>2</sup>

<sup>3</sup>*Galileo Galilei Institute for theoretical physics,*<sup>2</sup>

*Centro Nazionale INFN di Studi Avanzati Largo Enrico Fermi 2, I-50125, Firenze, Italy*<sup>2</sup>

<sup>4</sup>*Departament de Física, Universitat Autònoma de Barcelona, 08193 Bellaterra, Barcelona, Spain*<sup>3</sup>

<sup>5</sup>*Institut de Física d'Altes Energies (IFAE) and The Barcelona Institute of Science and Technology (BIST),*<sup>3</sup>

*Campus UAB, 08193 Bellaterra (Barcelona), Spain*<sup>3</sup>

We investigate the presence of extra relativistic degrees of freedom in the early Universe, contributing to the effective number of neutrinos  $N_{\text{eff}}$ , as  $\Delta N_{\text{eff}} \equiv N_{\text{eff}} - 3.044 > 0$ , in light of the recent measurements of Baryon Acoustic Oscillations (BAO) by the DESI collaboration. We analyze one-parameter extensions of the  $\Lambda$ CDM model where dark radiation (DR) is free streaming or behaves as a perfect fluid, due to self-interactions. We report a significant relaxation of upper bounds on  $\Delta N_{\text{eff}}$ , with respect to previous BAO data from SDSS+6dFGS, when additionally employing *Planck* data (and supernovae data from *Pantheon+*), setting  $\Delta N_{\text{eff}} \leq 0.39$  (95% C.L.) for free streaming DR, and a very mild preference for fluid DR,  $\Delta N_{\text{eff}} = 0.221^{+0.088}_{-0.18}$  ( $4 \leq 0.46$ , 95% C.L.). Applying constraints from primordial element abundances leads to slightly tighter constraints on  $\Delta N_{\text{eff}}$ , but they are avoided if DR is produced after Big Bang Nucleosynthesis (BBN). For fluid DR we estimate the tension with the SH<sub>0</sub>ES determination of  $H_0$  to be around  $(2.3 - 2.8)\sigma$  level, and for free-streaming DR the tension is below  $3\sigma$  if production occurs after BBN. This lesser degree of tension motivates a combination with SH<sub>0</sub>ES in these cases, resulting in a  $4.4\sigma - 5\sigma$  evidence for dark radiation with  $\Delta N_{\text{eff}} \simeq 0.6$  and large improvements in  $\chi^2$  over  $\Lambda$ CDM,  $-18 \lesssim \Delta\chi^2 \lesssim -25$ .<sup>4</sup>

## I. Introduction<sup>5</sup>

Modern cosmological datasets are among the most powerful probes of physics beyond the Standard Model (SM), even when this has negligible interactions with SM particles. This is particularly true if new physics is in the form of light degrees of freedom that remain ultra-relativistic throughout the cosmological evolution, until after the epoch of recombination. Their additional contribution to the energy density impacts the background expansion and density perturbations in the early Universe, when the Cosmic Microwave Background (CMB) is produced (see [1, 2] and [3]). Finding evidence for such *dark radiation* (DR), or alternatively constraining its presence to unprecedented levels, is one of the main targets of active and future cosmological surveys [4–9], and has a potentially groundbreaking impact on fundamental physics.<sup>6</sup>

The aim of this *Letter* is to assess the status of DR in light of the new measurements of Baryon Acoustic Oscillations (BAO) from galaxies and quasars [10] at redshifts  $0.3 \lesssim z \lesssim 1.5$  and from the Lyman- $\alpha$  forest [11] by the Dark Energy Spectroscopic Instrument [12] (DESI).<sup>7</sup>

BAO data from previous galactic surveys [13–15] have so far provided the most stringent constraints on

DR, when combined with CMB measurements from the Planck satellite [16] (Big Bang Nucleosynthesis and measurements of primordial element abundances provide an alternative probe, though one with possibly larger uncertainties, see e.g. the discussion in [17], and [18] for a recent update). In terms of the customary parameterization of the abundance of DR, given by the *effective number of neutrino species*, i.e.  $\Delta N_{\text{eff}} \equiv \rho_{\text{DR}}/\rho_\nu$ , where  $\rho_\nu$  is the energy density of a single neutrino species, the DESI collaboration has recently reported  $\Delta N_{\text{eff}} \leq 0.40$  (95% C.L.) [12] for free streaming species. Interestingly, this is a significant relaxation of the previous CMB+BAO bound  $\Delta N_{\text{eff}} \leq 0.28$  [16] (95% C.L., with fixed sum of neutrino masses  $\sum m_\nu = 0.06$  eV). Both these results were obtained allowing for  $\Delta N_{\text{eff}} < 0$  in the prior.<sup>8</sup>

While the  $\Delta N_{\text{eff}}$  parameterization effectively captures a vast landscape of particle physics scenarios, the specific microphysical origin of DR can lead to different imprints on cosmological observables. Perhaps the simplest model dependence arises between the case where DR is free streaming (some well motivated examples are: the QCD axion with a small mass [19–27] and relic gravitational waves, see also [28] for other candidates), and the possibility that it behaves as a perfect fluid with equation of state parameter  $w = 1/3$  (see e.g. the discussion in [3]). This latter case applies to a self-interacting gas of relativistic particles (as can arise e.g. in dark sector models with gauge interactions [29–31]), see [32–37] for investigations with previous data, and to scalar fields that start oscillating in quartic potentials well

\* itamar\_allali@brown.edu<sup>1</sup>

† notari@fqa.ub.edu

‡ frompineve@ifae.es

before recombination. A different simple scenario that is captured by  $\Delta N_{\text{eff}}$  is one where the abundance of neutrinos differs from the prediction of the SM, as can be the case if neutrinos or photons are slightly reheated by a dark sector after their decoupling (i.e. at temperatures below MeV).<sup>9</sup>

The first aim of this work is thus to provide the state-of-the-art constraints on such simplest DR scenarios, also accounting for data from additional cosmological observations, such as measurements of the Hubble diagram from supernovae [38] and of primordial element abundances. These can then be used by particle physicists to determine bounds on microphysical models.

Our findings then lead to the second aim of our work. We indeed interestingly find that the new BAO data allow for larger abundances of DR in all cases of study, which motivates a reassessment of whether such simple one parameter extensions of the  $\Lambda$ CDM model can reconcile the value of the Hubble expansion parameter  $H_0$  inferred from fitting to cosmological datasets, with the larger value measured from supernovae [39] (see also [40–42] for other measurements).<sup>11</sup>

## II. Models and datasets 17

We limit our study to the following three simple realizations of DR, all effectively captured by a single parameter  $\Delta N_{\text{eff}} \equiv N_{\text{eff}} - 3.044$ , where the latter contribution comes from SM neutrinos:<sup>18</sup>

- **Free-streaming:** these species, assumed to be massless, have large anisotropic stress [1] that produces a phase shift in CMB anisotropies.<sup>19</sup>
- **Fluid:** there is no anisotropic stress, thus the perturbation equations are the Euler and continuity equations of perfect adiabatic fluid with  $w = c_s^2 = 1/3$  [43]. The extra species is still assumed to be massless.<sup>19</sup>
- **Neutrinos:** we allow for the SM neutrino temperature to differ from that predicted by the SM (both larger or smaller), while keeping the free-streaming nature of neutrinos.<sup>19</sup>

The first two models have exactly the same background evolution, and differ only at the level of perturbations. While strictly speaking the species are described as massless, the  $\Delta N_{\text{eff}}$  parametrization effectively captures any scenario where the mass is somewhat below 0.05 eV.

The third model differs at both levels, since SM neutrinos have a non-negligible mass around and after recombination. Throughout our work, we take neutrinos to be degenerate in mass and temperature and impose the prior  $\sum m_\nu \geq 0.06$  eV from neutrino oscillations. We therefore always add  $\sum m_\nu$  as an additional free cosmological parameter to the  $\Lambda$ CDM model.<sup>1</sup> For the

first two models above, the neutrino sector is not altered with respect to the SM prediction, and thus a prior  $\Delta N_{\text{eff}} \geq 0$  is imposed.<sup>2</sup>

We perform Bayesian searches using CLASS [44, 45] to solve for the cosmological evolution and MontePython [46, 47] to collect Markov Chain Monte Carlo (MCMC) samples. We obtain posteriors and figures using GetDist [48]. We consider the following datasets in our searches:

- **P18:** Planck 2018 high- $\ell$  and low- $\ell$  TT, TE, EE and lensing data [17].
- **+DESI:** BAO measurements from DESI 2024 [12].
- **+SDSS+6dFGS.** BAO measurements from 6dFGS at  $z = 0.106$  [13], SDSS MGS at  $z = 0.15$  [14] (BAO smallz), and CMASS and LOWZ galaxy samples of BOSS DR12 at  $z = 0.38, 0.51$ , and  $0.61$  [49]. We use this only in alternative to DESI BAO data.
- **+Pantheon\_Plus.** The Pantheon+ supernovae compilation [38]. We use the Pantheon\_Plus likelihood in MontePython.
- **+Y<sub>He</sub>, D/H:** measurements of the abundance of primordial elements from [50] for Helium and [51] for Deuterium. The theoretical prediction for  $Y_{\text{He}}$  at BBN is determined using [52] and ParthenoPE v 1.10, as implemented in the likelihood bbn in MontePython.
- **+H<sub>0</sub>:** the latest measurement of the intrinsic SNIa magnitude  $M_b = -19.253 \pm 0.027$  from the SH0ES collaboration [39]. We add this only in combination with Pantheon+ data, as consistently implemented in the Pantheon\_Plus\_SH0ES likelihood in MontePython.

For the purposes of setting constraints, we will consider the combination **P18+DESI+Pantheon\_Plus** to be our baseline dataset (comparing also to the case with +DESI exchanged for +SDSS+6dFGS). Weaker bounds from **P18+DESI** alone are reported in App. B 1. The +Y<sub>He</sub>, D/H dataset is used to generate constraints when appropriate. And finally, the +H<sub>0</sub> dataset is used when interpreting the  $H_0$  tension as a moderate statistical fluctuation.

<sup>1</sup> This has however little impact on our results, as already discussed in [17].

<sup>2</sup> This differs from the choice of the DESI collaboration, the prior choice of which allows neutrinos to be colder than as predicted by the SM.

Parameter	P18+DESI+Pantheon.Plus			+Y <sub>He</sub> , D/H <sub>35</sub>	
	Free-streaming	Fluid	Neutrinos	Free-streaming	Fluid <sup>9</sup>
$\Delta N_{\text{eff}}$	$< 0.386$	$0.221^{+0.088}_{-0.18}$	$0.06^{+0.17}_{-0.19}$	$< 0.295$	$< 0.365$ <sup>13</sup>
$H_0$ [km/s/Mpc]	$68.79^{+0.60}_{-0.89}$ <sup>14</sup>	$69.35^{+0.81}_{-1.1}$	$68.0^{+1.0}_{-1.2}$ <sup>26</sup>	$68.62^{+0.53}_{-0.76}$	$68.97^{+0.65}_{-0.93}$
$H_0$ GT	$3.53\sigma$	$2.81\sigma$	$3.43\sigma$	$3.79\sigma$	$3.31\sigma$
$H_0$ IT	$3.06\sigma$	$2.52\sigma$	$3.24\sigma$	$3.4\sigma$	$2.93\sigma$

TABLE I: Marginalized posteriors for  $\Delta N_{\text{eff}}$  and  $H_0$ . Two models for dark radiation are considered: free-streaming and perfect fluid. We report results with our baseline dataset, and additionally adding measurements of primordial abundances. We report upper bounds on  $\Delta N_{\text{eff}}$  at 95% C.L. for all models and datasets, except for the fluid model fitted to the baseline dataset, where a  $1\sigma$  preference for dark radiation is found (the 95% C.L. upper bound is  $\Delta N_{\text{eff}} < 0.461$ ). The corresponding tension with the SH<sub>0</sub>ES measurement is also reported. Posteriors for all parameters are reported in Appendices B 2 and B 5 for the baseline and +Y<sub>He</sub>, D/H datasets, respectively.

### III. New constraints on dark radiation<sup>25</sup>

Let us first focus on the impact of the new BAO data from DESI on DR models. We fit the models of free-streaming and fluid DR to the baseline dataset, and compare this to the case where previous BAO data are used instead of DESI BAO. Posteriors for  $\Delta N_{\text{eff}}$  and  $H_0$  are shown in Fig. 1. One can immediately appreciate the qualitative difference in the results: for both free-streaming and fluid DR, the  $1$  and  $2\sigma$  regions of the posteriors extend to larger values of  $\Delta N_{\text{eff}}$ , indicating that the DESI BAO data allow for larger abundances of DR. The new 95% C.L. constraints are reported in Table I, and show a significant relaxation of up to 20% for free-streaming DR with respect to using +SDSS+6dFGS, see Appendix B 7 (our 95% C.L. upper bound on  $\Delta N_{\text{eff}}$  agrees with [12], despite our different prior choice; the central value is however shifted to larger values than in [12], as expected). The situation is even more interesting for the fluid DR scenario: the 1d marginalized posterior for  $\Delta N_{\text{eff}}$  is shifted to larger values, and a non vanishing abundance  $\Delta N_{\text{eff}} \approx 0.2$  is now (very mildly) preferred at  $1\sigma$ . We report further posteriors in Table I. In particular, for the neutrino model we find that deviations of up to 6% from the SM abundance are allowed. In all our runs we find similar upper bounds  $m_\nu \leq 0.12 \sim 0.13$  eV. Full posteriors for all models and cosmological parameters are reported in Appendix B.

The DR abundance allowed by the new BAO data is potentially independently constrained by observations of light element abundances. We therefore examine the impact of these measurements using the +Y<sub>He</sub>, D/H dataset. We report the resulting upper bounds on  $\Delta N_{\text{eff}}$  in Table I. One can see that the mild preference for  $\Delta N_{\text{eff}} > 0$  in the fluid case is erased by the +Y<sub>He</sub>, D/H data. Constraints on  $\Delta N_{\text{eff}}$  become significantly tighter for the free-streaming case as well.

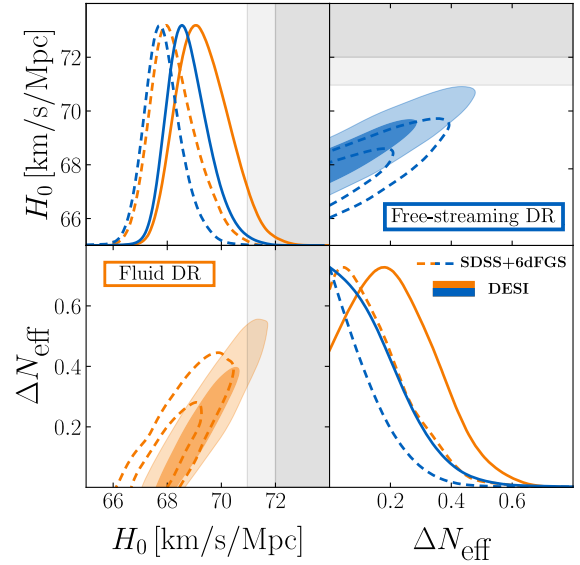


FIG. 1: 1- and 2-d posterior distributions for  $H_0$  and  $\Delta N_{\text{eff}}$  in dark radiation models, obtained using our baseline dataset. We compare our results with the new DESI BAO data (solid curves/shaded contours) with those obtained with previous BAO data (dashed curves/contours).

Note that measurements of primordial elements exist, which disagree with those that we have used (see e.g. [16, 53] for a summary). For instance, using [54] rather than [50] would lead to significant evidence for  $\Delta N_{\text{eff}}$  (as noted similarly for free streaming DR in [16, 55]).

We now move to  $H_0$ , and highlight two interesting effects of the new BAO data: first, larger values are preferred, even in the absence of dark radiation. Second, the alleviated constraints on  $\Delta N_{\text{eff}}$  allow for even larger values of  $H_0$ , given the strong degeneracy between these two parameters. For comparison, the SH<sub>0</sub>ES measurement is shown by the gray shaded bands ( $1-$  and  $2\sigma$ ) in Fig. 1. Within the context of fluid DR,

<sup>3</sup> We do not highlight here the results for neutrinos (see however Appendix B 5), since modifying the neutrino abundance can most plausibly be achieved after BBN.

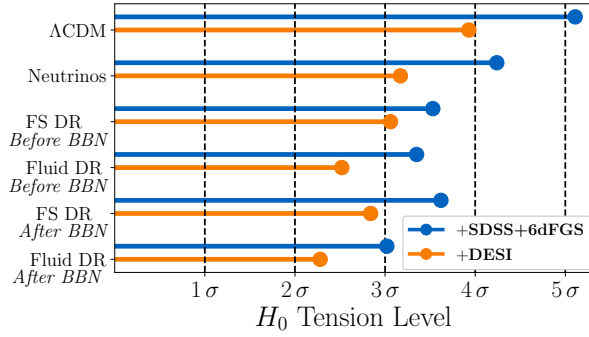


FIG. 2: Measure of the tension (IT, see Appendix A) in the determinations of  $H_0$  from the **P18+DESI+Pantheon+Plus** dataset with respect to the  $SH_0ES$  measurement, for models considered in this work. Results with previous BAO data are shown for comparison.

as can be also appreciated in Fig. 1. We report two measures of tension in Table I: one based on a simple Gaussian estimate (GT) which is commonly employed in the literature but leads to overestimates when the posteriors are asymmetric, as in our case; the second measure partially corrects for this by using the true posterior distribution from our MCMC analysis (IT), as suggested in [56] and reviewed in Appendix A. We estimate the tension to be around  $2.5\sigma$  within the fluid model, and around  $3\sigma$  in the free-streaming scenario, when we do not include constraints from primordial elements (the tension is further lowered by  $\sim 0.3\sigma$  using **P18+DESI** alone, see App. B1). These results represent a significant alleviation of the  $H_0$  tension within these models. Comparing to results obtained with previous BAO data, we find that DESI reduces the tension by  $(0.5 - 1)\sigma$  depending on the model, see Fig. 2. The  $\Delta\chi^2$  for all models and datasets considered here with respect to  $\Lambda$ CDM is close to zero.

#### IV. The Hubble tension

Our findings (especially for the fluid DR model) open the possibility to interpret the Hubble tension as a mild to moderate statistical fluctuation within the context of the  $\Lambda$ CDM +  $\Delta N_{\text{eff}}$  models presented above.

Additional constraints from primordial elements from [50, 51] worsen the tension in all models. However, they are avoided if the dark radiation is produced after the epoch of BBN and sufficiently before recombination. This specification does not introduce any additional parameters, nor does it lead to a coincidence problem (in contrast to models where a fluid is taken to undergo a transition around the epoch of recombination, such as [57–61]), since DR can still be produced in a redshift range that spans around five orders of magnitude, corresponding to  $\text{eV} \lesssim T \lesssim 100 \text{ keV}$ .

Beside the relevance of primordial element constraints, a difference arises if DR is indeed produced after BBN, compared to the previous case which implicitly assumed production before BBN. In the latter case, DR alters the theoretical prediction of  $Y_{\text{He}}$ , which then affects the number density of electrons at recombination  $n_e(z) \propto (1 - Y_{\text{He}})$  (see e.g. [62] for a recent discussion). Therefore, when considering the scenario where DR is produced after BBN, we determine  $Y_{\text{He}}$  by setting  $\Delta N_{\text{eff}} = 0$  at BBN. We compare the inferences made with our baseline dataset for both fluid and free-streaming DR produced after BBN in Table II. Interestingly, we find an additional reduction of the  $H_0$  tension (and relaxation of constraints on  $\Delta N_{\text{eff}}$ ), and a  $\gtrsim 1\sigma$  preference for fluid DR persists.

Having estimated the tension in DR models with production after BBN to be around  $(2.3 - 2.8)\sigma$  compared to the  $\Lambda$ CDM model, we combine our baseline dataset with the  $SH_0ES$  determination of  $H_0$ . Results are presented in the rightmost columns of Table II. Remarkably, we find evidence at the  $5\sigma$  ( $4.5\sigma$ ) level for fluid (free-streaming) DR, and a negligible residual tension with  $SH_0ES$ . This is accompanied by a very significant improvement in  $\chi^2$  with respect to the  $\Lambda$ CDM model. We account for the additional parameter via the Akaike Information Criterion (AIC) [63] (see also [64])  $\Delta\text{AIC} \equiv \Delta\chi^2 + 2 \times (\# \text{ of added free parameters})$  and report  $\Delta\text{AIC} \simeq -23(-19)$  for fluid (free-streaming) DR.

In all the models and combination of datasets used in this work, we find posteriors for the matter clustering parameter  $S_8 \equiv \sigma_8 \sqrt{\Omega_m/0.3}$  in agreement with the most recent measurements from weak lensing surveys [65].

Finally, we have focused here on perhaps the simplest DR scenarios, but it is conceivable that analogous conclusions could apply to other scenarios that lead to a similar evolution for the cosmological background, for instance models with varying Newton constant, see e.g. [66].

#### V. Discussion

The large improvements in the goodness-of-the-fit which we find are of course driven by the  $SH_0ES$  measurement, and have been reported to a similar level in the past for other models with previous BAO data. Therefore, one may doubt the relevance of our results. However, we would like to stress two crucial differences with such previous findings. First, our results are obtained by combining datasets that are in  $\sim 2.5\sigma$  tension with each other within the context of DR models when production occurs only after BBN, especially for the fluid DR case (removing Pantheon+ data further reduces the tension to even  $\sim 2\sigma$ , see Appendix B1). Second, the models under consideration are simple, one-parameter extensions of  $\Lambda$ CDM, with several possible implementations in particle physics.

Perhaps the simplest example of DR production after BBN, which can arise in a broad class of models, is a



Parameter	P18+DESI+Pantheon.Plus		+H <sub>0</sub> 35	
	Free-streaming DR	Fluid DR	Free-streaming DR	Fluid DR 34
$\Delta N_{\text{eff}}$	$< 0.435$	$0.26 (0.34)^{+0.11}_{-0.21}$	$0.63 (0.56) \pm 0.14$	$0.65 (0.73) \pm 0.13$
$H_0$ [km/s/Mpc]	$68.94 (68.41)^{+0.63}_{-0.99}$ 46	$69.56 (69.82)^{+0.85}_{-1.2}$	$71.82 (71.65)^{+0.78}_{-0.77}$	$72.26 (73.0)^{+0.77}_{-0.78}$
$H_0$ GT	$3.37\sigma$	$2.59\sigma$	$0.94\sigma$	$0.6\sigma$
$H_0$ IT	$2.84\sigma$	$2.28\sigma$	$0.94\sigma$	$0.6\sigma$
$\Delta\chi^2$	$\sim 0$	$-0.4$	$-20.5$	$-24.7$
$\Delta\text{AIC}$	$+2.0$	$+1.6$	$-18.5$	$-22.7$

TABLE II: Marginalized posteriors for  $\Delta N_{\text{eff}}$  and  $H_0$  for scenarios where dark radiation is produced after BBN. Two models are considered: free-streaming and fluid DR. We report results with our baseline dataset, and additionally adding the determination of  $H_0$  from SH<sub>0</sub>ES. The corresponding tension with the SH<sub>0</sub>ES measurement is also reported, as well as two measures of goodness-of-fit compared to the  $\Lambda$ CDM model. Posteriors for all parameters are reported in Appendices B 8 and B 9. 38

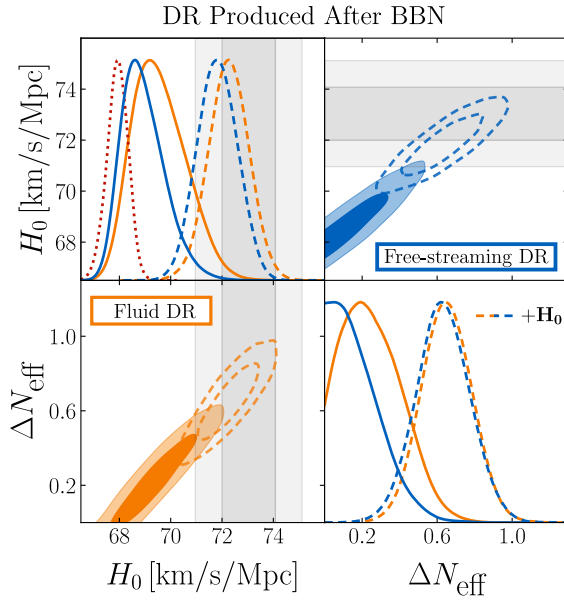


FIG. 3: 1- and 2-d posterior distributions for  $H_0$  and  $\Delta N_{\text{eff}}$  in models with dark radiation produced after BBN. We compare our results obtained with our baseline dataset (solid curves/shaded contours) with those obtained by combining with the determination of  $H_0$  from SH<sub>0</sub>ES (dashed curves/contours). The 1-d  $H_0$  posterior for  $\Lambda$ CDM with the baseline dataset is shown by the dotted curve. 38

massive particle, the abundance of which is negligible in the pre-BBN era, and that decays to some light states after BBN (see e.g. [67–72]), with a decay rate  $10^{-37} \text{ GeV} \lesssim \Gamma \lesssim 10^{-27} \text{ GeV}$ . Other possibilities exist in the literature for the production of DR after BBN; see,

for instance, [73, 74]. 47

Our work provides new state-of-the-art bounds on dark radiation models, that partially relax constraints on beyond the SM physics and should prove important for model building. 48

Remarkably, our findings also suggest that the new BAO data open the possibility to address the Hubble tension with well-motivated minimal extensions of  $\Lambda$ CDM model. 4

With a conservative perspective, the possibility that our findings are driven by a statistical fluctuation or underestimated systematic uncertainties in the DESI measurement (which exhibit some discrepancy with previous BAO data) should be kept in mind, and will be decisively clarified soon by upcoming data releases from DESI itself and Euclid, see e.g. [75], where the  $1\sigma$  error on  $\Delta N_{\text{eff}}$  for the free streaming case from Euclid power spectrum and lensing measurements is forecasted to be 0.05. 50

## Acknowledgments

We thank Héctor Gil-Marín for help with DESI data. The work of F.R. is supported by the grant RYC2021-031105-I from the Ministerio de Ciencia e Innovación (Spain). I.J.A. is supported by NASA grant 80NSSC22K081. The work of A.N. is supported by the grants PID2019-108122GB-C32 from the Spanish Ministry of Science and Innovation, Unit of Excellence Maria de Maeztu 2020-2023 of ICCUB (CEX2019-000918-M) and AGAUR 2021 SGR 00872. A.N. is grateful to the Physics Department of the University of Florence for the hospitality during the course of this work. We acknowledge use of the Tufts HPC research cluster and the INFN Florence cluster. 51

[1] S. Bashinsky and U. Seljak, Neutrino perturbations in CMB anisotropy and matter clustering, *Phys. Rev. D* 6

69, 083002 (2004), arXiv:astro-ph/0310198.

- [2] Z. Hou, R. Keisler, L. Knox, M. Millea, and C. Reichardt, How Massless Neutrinos Affect the Cosmic Microwave Background Damping Tail, *Phys. Rev. D* **87**, 083008 (2013), arXiv:1104.2333 [astro-ph.CO].
- [3] D. Baumann, D. Green, J. Meyers, and B. Wallisch, Phases of New Physics in the CMB, *JCAP* **01**, 007, arXiv:1508.06342 [astro-ph.CO].
- [4] S. Aiola *et al.* (ACT), The Atacama Cosmology Telescope: DR4 Maps and Cosmological Parameters, *JCAP* **12**, 047, arXiv:2007.07288 [astro-ph.CO].
- [5] J. A. Sobrin *et al.* (SPT-3G), The Design and Integrated Performance of SPT-3G, *Astrophys. J. Supp.* **258**, 42 (2022), arXiv:2106.11202 [astro-ph.IM].
- [6] L. Amendola *et al.*, Cosmology and fundamental physics with the Euclid satellite, *Living Rev. Rel.* **21**, 2 (2018), arXiv:1606.00180 [astro-ph.CO].
- [7] v. Ivezić *et al.* (LSST), LSST: from Science Drivers to Reference Design and Anticipated Data Products, *Astrophys. J.* **873**, 111 (2019), arXiv:0805.2366 [astro-ph].
- [8] K. Abazajian *et al.* (CMB-S4), Snowmass 2021 CMB-S4 White Paper, (2022), arXiv:2203.08024 [astro-ph.CO].
- [9] P. Ade *et al.* (Simons Observatory), The Simons Observatory: Science goals and forecasts, *JCAP* **02**, 056, arXiv:1808.07445 [astro-ph.CO].
- [10] A. G. Adame *et al.* (DESI), DESI 2024 III: Baryon Acoustic Oscillations from Galaxies and Quasars, (2024), arXiv:2404.03000 [astro-ph.CO].
- [11] A. G. Adame *et al.* (DESI), DESI 2024 IV: Baryon Acoustic Oscillations from the Lyman Alpha Forest, (2024), arXiv:2404.03001 [astro-ph.CO].
- [12] A. G. Adame *et al.* (DESI), DESI 2024 VI: Cosmological Constraints from the Measurements of Baryon Acoustic Oscillations, (2024), arXiv:2404.03002 [astro-ph.CO].
- [13] F. Beutler, C. Blake, M. Colless, D. H. Jones, L. Staveley-Smith, L. Campbell, Q. Parker, W. Saunders, and F. Watson, The 6dF Galaxy Survey: Baryon Acoustic Oscillations and the Local Hubble Constant, *Mon. Not. Roy. Astron. Soc.* **416**, 3017 (2011), arXiv:1106.3366 [astro-ph.CO].
- [14] A. J. Ross, L. Samushia, C. Howlett, W. J. Percival, A. Burden, and M. Manera, The clustering of the SDSS DR7 main Galaxy sample – I. A 4 per cent distance measure at  $z = 0.15$ , *Mon. Not. Roy. Astron. Soc.* **449**, 835 (2015), arXiv:1409.3242 [astro-ph.CO].
- [15] S. Satpathy *et al.* (BOSS), The clustering of galaxies in the completed SDSS-III Baryon Oscillation Spectroscopic Survey: On the measurement of growth rate using galaxy correlation functions, *Mon. Not. Roy. Astron. Soc.* **469**, 1369 (2017), arXiv:1607.03148 [astro-ph.CO].
- [16] N. Aghanim *et al.* (Planck), Planck 2018 results. VI. Cosmological parameters, *Astron. Astrophys.* **641**, A6 (2020), [Erratum: *Astron. Astrophys.* 652, C4 (2021)], arXiv:1807.06209 [astro-ph.CO].
- [17] N. Aghanim *et al.* (Planck), Planck 2018 results. V. CMB power spectra and likelihoods, *Astron. Astrophys.* **641**, A5 (2020), arXiv:1907.12875 [astro-ph.CO].
- [18] T.-H. Yeh, J. Shelton, K. A. Olive, and B. D. Fields, Probing physics beyond the standard model: limits from BBN and the CMB independently and combined, *JCAP* **10**, 046, arXiv:2207.13133 [astro-ph.CO].
- [19] M. S. Turner, Thermal Production of Not SO Invisible Axions in the Early Universe, *Phys. Rev. Lett.* **59**, 2489 (1987), [Erratum: *Phys. Rev. Lett.* 60, 1101 (1988)].
- [20] E. W. Kolb and M. S. Turner, *The Early Universe*, Vol. 69 (1990).
- [21] Z. G. Berezhiani, A. S. Sakharov, and M. Y. Khlopov, Primordial background of cosmological axions, *Sov. J. Nucl. Phys.* **55**, 1063 (1992).
- [22] S. Chang and K. Choi, Hadronic axion window and the big bang nucleosynthesis, *Phys. Lett. B* **316**, 51 (1993), arXiv:hep-ph/9306216.
- [23] E. Masso, F. Rota, and G. Zsembinszki, On axion thermalization in the early universe, *Phys. Rev. D* **66**, 023004 (2002), arXiv:hep-ph/0203221.
- [24] R. Z. Ferreira, A. Notari, and F. Rompineve, Dine-Fischler-Srednicki-Zhitnitsky axion in the CMB, *Phys. Rev. D* **103**, 063524 (2021), arXiv:2012.06566 [hep-ph].
- [25] A. Notari, F. Rompineve, and G. Villadoro, Improved Hot Dark Matter Bound on the QCD Axion, *Phys. Rev. Lett.* **131**, 011004 (2023), arXiv:2211.03799 [hep-ph].
- [26] F. D’Eramo, R. Z. Ferreira, A. Notari, and J. L. Bernal, Hot Axions and the  $H_0$  tension, *JCAP* **11**, 014, arXiv:1808.07430 [hep-ph].
- [27] R. Z. Ferreira and A. Notari, Observable Windows for the QCD Axion Through the Number of Relativistic Species, *Phys. Rev. Lett.* **120**, 191301 (2018), arXiv:1801.06090 [hep-ph].
- [28] D. Baumann, D. Green, and B. Wallisch, New Target for Cosmic Axion Searches, *Phys. Rev. Lett.* **117**, 171301 (2016), arXiv:1604.08614 [astro-ph.CO].
- [29] Z. Chacko, Y. Cui, S. Hong, and T. Okui, Hidden dark matter sector, dark radiation, and the CMB, *Phys. Rev. D* **92**, 055033 (2015), arXiv:1505.04192 [hep-ph].
- [30] M. A. Buen-Abad, G. Marques-Tavares, and M. Schmaltz, Non-Abelian dark matter and dark radiation, *Phys. Rev. D* **92**, 023531 (2015), arXiv:1505.03542 [hep-ph].
- [31] Z. Chacko, Y. Cui, S. Hong, T. Okui, and Y. Tsai, Partially Acoustic Dark Matter, Interacting Dark Radiation, and Large Scale Structure, *JHEP* **12**, 108, arXiv:1609.03569 [astro-ph.CO].
- [32] F.-Y. Cyr-Racine, K. Sigurdson, J. Zavala, T. Bringmann, M. Vogelsberger, and C. Pfrommer, ETHOS—an effective theory of structure formation: From dark particle physics to the matter distribution of the Universe, *Phys. Rev. D* **93**, 123527 (2016), arXiv:1512.05344 [astro-ph.CO].
- [33] J. Lesgourgues, G. Marques-Tavares, and M. Schmaltz, Evidence for dark matter interactions in cosmological precision data?, *JCAP* **02**, 037, arXiv:1507.04351 [astro-ph.CO].
- [34] C. Brust, Y. Cui, and K. Sigurdson, Cosmological Constraints on Interacting Light Particles, *JCAP* **08**, 020, arXiv:1703.10732 [astro-ph.CO].
- [35] M. A. Buen-Abad, M. Schmaltz, J. Lesgourgues, and T. Brinckmann, Interacting Dark Sector and Precision Cosmology, *JCAP* **01**, 008, arXiv:1708.09406 [astro-ph.CO].
- [36] M. Archidiacono, D. C. Hooper, R. Murgia, S. Bohr, J. Lesgourgues, and M. Viel, Constraining Dark Matter–Dark Radiation interactions with CMB, BAO, and Lyman- $\alpha$ , *JCAP* **10**, 055, arXiv:1907.01496 [astro-ph.CO].
- [37] N. Blinov and G. Marques-Tavares, Interacting radiation after Planck and its implications for the Hubble Tension, *JCAP* **09**, 029, arXiv:2003.08387 [astro-ph.CO].
- [38] D. Scolnic *et al.*, The Pantheon+ Analysis: The Full

- Data Set and Light-curve Release, *Astrophys. J.* **938**, 113 (2022), arXiv:2112.03863 [astro-ph.CO].
- [39] A. G. Riess *et al.*, A Comprehensive Measurement of the Local Value of the Hubble Constant with  $1 \text{ km s}^{-1} \text{ Mpc}^{-1}$  Uncertainty from the Hubble Space Telescope and the SH0ES Team, *Astrophys. J. Lett.* **934**, L7 (2022), arXiv:2112.04510 [astro-ph.CO].
- [40] K. C. Wong *et al.*, H0LiCOW – XIII. A 2.4 per cent measurement of  $H_0$  from lensed quasars:  $5.3\sigma$  tension between early- and late-Universe probes, *Mon. Not. Roy. Astron. Soc.* **498**, 1420 (2020), arXiv:1907.04869 [astro-ph.CO].
- [41] D. Scolnic, A. G. Riess, J. Wu, S. Li, G. S. Anand, R. Beaton, S. Casertano, R. I. Anderson, S. Dhawan, and X. Ke, CATS: The Hubble Constant from Standardized TRGB and Type Ia Supernova Measurements, *Astrophys. J. Lett.* **954**, L31 (2023), arXiv:2304.06693 [astro-ph.CO].
- [42] W. L. Freedman, Measurements of the Hubble Constant: Tensions in Perspective, *Astrophys. J.* **919**, 16 (2021), arXiv:2106.15656 [astro-ph.CO].
- [43] C.-P. Ma and E. Bertschinger, Cosmological perturbation theory in the synchronous and conformal Newtonian gauges, *Astrophys. J.* **455**, 7 (1995), arXiv:astro-ph/9506072.
- [44] J. Lesgourgues, The Cosmic Linear Anisotropy Solving System (CLASS) I: Overview, (2011), arXiv:1104.2932 [astro-ph.IM].
- [45] D. Blas, J. Lesgourgues, and T. Tram, The Cosmic Linear Anisotropy Solving System (CLASS) II: Approximation schemes, *JCAP* **07**, 034, arXiv:1104.2933 [astro-ph.CO].
- [46] B. Audren, J. Lesgourgues, K. Benabed, and S. Prunet, Conservative Constraints on Early Cosmology: an illustration of the Monte Python cosmological parameter inference code, *JCAP* **02**, 001, arXiv:1210.7183 [astro-ph.CO].
- [47] T. Brinckmann and J. Lesgourgues, MontePython 3: boosted MCMC sampler and other features, *Phys. Dark Univ.* **24**, 100260 (2019), arXiv:1804.07261 [astro-ph.CO].
- [48] A. Lewis, GetDist: a Python package for analysing Monte Carlo samples, (2019), arXiv:1910.13970 [astro-ph.IM].
- [49] S. Alam *et al.* (BOSS), The clustering of galaxies in the completed SDSS-III Baryon Oscillation Spectroscopic Survey: cosmological analysis of the DR12 galaxy sample, *Mon. Not. Roy. Astron. Soc.* **470**, 2617 (2017), arXiv:1607.03155 [astro-ph.CO].
- [50] E. Aver, K. A. Olive, and E. D. Skillman, The effects of He I  $\lambda 10830$  on helium abundance determinations, *JCAP* **07**, 011, arXiv:1503.08146 [astro-ph.CO].
- [51] R. J. Cooke, M. Pettini, and C. C. Steidel, One Percent Determination of the Primordial Deuterium Abundance, *Astrophys. J.* **855**, 102 (2018), arXiv:1710.11129 [astro-ph.CO].
- [52] L. E. Marcucci, G. Mangano, A. Kievsky, and M. Viviani, Implication of the proton-deuteron radiative capture for Big Bang Nucleosynthesis, *Phys. Rev. Lett.* **116**, 102501 (2016), [Erratum: *Phys. Rev. Lett.* **117**, 049901 (2016)], arXiv:1510.07877 [nucl-th].
- [53] E. Aver, D. A. Berg, K. A. Olive, R. W. Pogge, J. J. Salzer, and E. D. Skillman, Improving helium abundance determinations with Leo P as a case study, *JCAP* **03**, 027, arXiv:2010.04180 [astro-ph.CO].
- [54] Y. I. Izotov, T. X. Thuan, and N. G. Guseva, A new determination of the primordial He abundance using the He I  $\lambda 10830 \text{ \AA}$  emission line: cosmological implications, *Mon. Not. Roy. Astron. Soc.* **445**, 778 (2014), arXiv:1408.6953 [astro-ph.CO].
- [55] N. Schöneberg, J. Lesgourgues, and D. C. Hooper, The BAO+BBN take on the Hubble tension, *JCAP* **10**, 029, arXiv:1907.11594 [astro-ph.CO].
- [56] M. Raveri and C. Doux, Non-Gaussian estimates of tensions in cosmological parameters, *Phys. Rev. D* **104**, 043504 (2021), arXiv:2105.03324 [astro-ph.CO].
- [57] V. Poulin, T. L. Smith, T. Karwal, and M. Kamionkowski, Early Dark Energy Can Resolve The Hubble Tension, *Phys. Rev. Lett.* **122**, 221301 (2019), arXiv:1811.04083 [astro-ph.CO].
- [58] F. Niedermann and M. S. Sloth, New early dark energy, *Phys. Rev. D* **103**, L041303 (2021), arXiv:1910.10739 [astro-ph.CO].
- [59] M. Gonzalez, M. P. Hertzberg, and F. Rompineve, Ultralight Scalar Decay and the Hubble Tension, *JCAP* **10**, 028, arXiv:2006.13959 [astro-ph.CO].
- [60] I. J. Allali, M. P. Hertzberg, and F. Rompineve, Dark sector to restore cosmological concordance, *Phys. Rev. D* **104**, L081303 (2021), arXiv:2104.12798 [astro-ph.CO].
- [61] D. Aloni, A. Berlin, M. Joseph, M. Schmaltz, and N. Weiner, A Step in understanding the Hubble tension, *Phys. Rev. D* **105**, 123516 (2022), arXiv:2111.00014 [astro-ph.CO].
- [62] F.-Y. Cyr-Racine, F. Ge, and L. Knox, Symmetry of Cosmological Observables, a Mirror World Dark Sector, and the Hubble Constant, *Phys. Rev. Lett.* **128**, 201301 (2022), arXiv:2107.13000 [astro-ph.CO].
- [63] H. Akaike, A new look at the statistical model identification, *IEEE Transactions on Automatic Control* **19**, 716 (1974).
- [64] A. R. Liddle, Information criteria for astrophysical model selection, *Mon. Not. Roy. Astron. Soc.* **377**, L74 (2007), arXiv:astro-ph/0701113.
- [65] T. M. C. Abbott *et al.* (Kilo-Degree Survey, Dark Energy Survey), DES Y3 + KiDS-1000: Consistent cosmology combining cosmic shear surveys, *Open J. Astrophys.* **6**, 2305.17173 (2023), arXiv:2305.17173 [astro-ph.CO].
- [66] G. Ballesteros, A. Notari, and F. Rompineve, The  $H_0$  tension:  $\Delta G_N$  vs.  $\Delta N_{\text{eff}}$ , *JCAP* **11**, 024, arXiv:2004.05049 [astro-ph.CO].
- [67] K. Ichikawa, M. Kawasaki, K. Nakayama, M. Senami, and F. Takahashi, Increasing effective number of neutrinos by decaying particles, *JCAP* **05**, 008, arXiv:hep-ph/0703034.
- [68] W. Fischler and J. Meyers, Dark Radiation Emerging After Big Bang Nucleosynthesis?, *Phys. Rev. D* **83**, 063520 (2011), arXiv:1011.3501 [astro-ph.CO].
- [69] D. Hooper, F. S. Queiroz, and N. Y. Gnedin, Non-Thermal Dark Matter Mimicking An Additional Neutrino Species In The Early Universe, *Phys. Rev. D* **85**, 063513 (2012), arXiv:1111.6599 [astro-ph.CO].
- [70] O. E. Bjælde, S. Das, and A. Moss, Origin of  $\Delta N_{\text{eff}}$  as a Result of an Interaction between Dark Radiation and Dark Matter, *JCAP* **10**, 017, arXiv:1205.0553 [astro-ph.CO].
- [71] K. Choi, K.-Y. Choi, and C. S. Shin, Dark radiation and small-scale structure problems with decaying particles, *Phys. Rev. D* **86**, 083529 (2012), arXiv:1208.2496 [hep-ph].
- [72] J. Hasenkamp and J. Kersten, Dark radiation

- from particle decay: cosmological constraints and opportunities, *JCAP* **08**, 024, arXiv:1212.4160 [hep-ph]. 213
- [73] R. Z. Ferreira, A. Notari, O. Pujolas, and F. Rompineve, Gravitational waves from domain walls in Pulsar Timing Array datasets, *JCAP* **02**, 001, arXiv:2204.04228 [astro-ph.CO]. 214
- [74] D. Aloni, M. Joseph, M. Schmaltz, and N. Weiner, Dark Radiation from Neutrino Mixing after Big Bang Nucleosynthesis, *Phys. Rev. Lett.* **131**, 221001 (2023), arXiv:2301.10792 [astro-ph.CO]. 215
- [75] T. Brinckmann, D. C. Hooper, M. Archidiacono, J. Lesgourgues, and T. Sprenger, The promising future of a robust cosmological neutrino mass measurement, *JCAP* **01**, 059, arXiv:1808.05955 [astro-ph.CO]. 216
- [76] I. J. Allali, F. Rompineve, and M. P. Hertzberg, Dark sectors with mass thresholds face cosmological datasets, *Phys. Rev. D* **108**, 023527 (2023), arXiv:2305.14166 [astro-ph.CO]. 217
-



## Appendix 52

### A. Tension Measures 53

For the assessment of tension between the  $H_0$  measurement of the SH<sub>0</sub>ES collaboration and the inferences made in this work, we define the following metrics. First, the commonly used measure of “Gaussian tension” ( $GT$ ) is defined as 54

$$GT = \frac{|\mu_m - \mu_{MC}|}{\sqrt{\sigma_m^2 + \sigma_{MC}^2}} \quad (A1) \quad 117$$

where  $\mu_m$  and  $\mu_{MC}$  are the mean values of  $H_0$  determined by the SH<sub>0</sub>ES collaboration and by our MCMC analyses, respectively.  $\sigma_m^2$  is the variance for the SH<sub>0</sub>ES measurement. For the variance of the MCMC inference  $\sigma_{MC}^2$  we take the upper  $1\sigma$  error derived from our marginalized posteriors on  $H_0$ . Since the posteriors for  $H_0$  we derive are not symmetric, there is not a clear choice of whether to average the upper and lower  $\sigma$ , or to take the value that is on the side of the distribution closest to the SH<sub>0</sub>ES measurement (upper). In this work, we take  $\sigma_{MC}$  to always be the upper derived  $\sigma$  such that we do not underestimate the tension. 56

To address the non-gaussian nature of our inferred posteriors, we employ also the measure which we term the “integrated tension” ( $IT$ ) [56, 76], defined via 57

$$\int_{-\infty}^{\infty} \mathcal{P}_{MC}(h) \frac{1}{2} \left( 1 \pm \operatorname{erf} \left( \frac{h - \mu_m}{\sqrt{2}\sigma_m} \right) \right) dh \stackrel{IT}{=} \int_{-\infty}^{\infty} \frac{1}{\sqrt{2\pi}} e^{-\frac{1}{2}x^2} dx \quad (A2)$$

To understand this formula, let us examine each side. The left hand side is the integral over the cross-correlation of the two posterior distributions, namely the posterior distribution derived from our MCMC  $\mathcal{P}_{MC}(h)$ , and the posterior from the SH<sub>0</sub>ES measurement. In Eq. (A2), we have already integrated the SH<sub>0</sub>ES posterior, assuming it to be purely gaussian, and therefore all that remains are the mean and standard deviation  $\mu_m$  and  $\sigma_m$ . Using the posterior distribution from a given MCMC, the left hand side constitutes a probability (understood as the probability of measuring the SH<sub>0</sub>ES value given the posterior from MCMC). Then, the right hand side of Eq. (A2) equates this probability with the integral over a gaussian (with mean= 0 and variance= 1), and one solves for the upper limit of the integral  $IT$  which gives this same probability. For example, if the left hand side of Eq. (A2) gives a probability of 68%, then we obtain the measure of tension to be  $IT = 1\sigma$ . 59

### B. Detailed Posteriors 60

We present in the following sections the detailed posteriors we obtain when evaluating the several models discussed in this work against several combinations of datasets. Appendices B 1 to B 7 present tables and plots of posteriors for the models:  $\Lambda$ CDM, Free-streaming dark radiation, Fluid dark radiation, and Neutrinos. The title of each section gives the combination of data explored in that section. Then, Appendix B 8 and Appendix B 9 explore the posteriors with a variety of datasets on the models of dark radiation produced after BBN for fluid and free-streaming, respectively. 61

## 1. P18+DESI 23

Parameter	$\Lambda$ CDM	Free-streaming DR	Fluid DR	Neutrinos 26
$100\omega_b$	2.249 (2.248) $^{+0.013}_{-0.013}$	2.262 (2.264) $^{+0.016}_{-0.016}$	2.272 (2.274) $^{+0.017}_{-0.017}$	2.256 (2.25) $^{+0.019}_{-0.017}$
$\omega_{cdm}$	0.11811 (0.11823) $^{+0.00087}_{-0.00086}$	0.1208 (0.1212) $^{+0.0015}_{-0.0024}$	0.1224 (0.1205) $^{+0.0021}_{-0.0031}$	0.1193 (0.1176) $^{+0.0024}_{-0.0028}$
$\ln 10^{10} A_s$	3.054 (3.057) $^{+0.014}_{-0.016}$	3.062 (3.055) $^{+0.015}_{-0.017}$	3.052 (3.041) $^{+0.015}_{-0.016}$	3.058 (3.057) $^{+0.015}_{-0.018}$
$n_s$	0.9689 (0.9689) $^{+0.0036}_{-0.0036}$	0.9748 (0.9742) $^{+0.0047}_{-0.0057}$	0.9712 (0.9678) $^{+0.0039}_{-0.0039}$	0.9713 (0.9715) $^{+0.0064}_{-0.0065}$
$\tau_{reio}$	0.0608 (0.0608) $^{+0.0070}_{-0.0081}$	0.0614 (0.0595) $^{+0.0072}_{-0.0083}$	0.0619 (0.053) $^{+0.0072}_{-0.0084}$	0.0615 (0.0641) $^{+0.0067}_{-0.0087}$
$\Delta N_{eff}$	—	$< 0.395$	$0.25 (0.13)^{+0.11}_{-0.18}$	$0.12 (0.062)^{+0.16}_{-0.16}$
$\sum m_\nu$	$< 0.119$	$< 0.124$	$< 0.127$	$< 0.116$ 65
$H_0$ [km/s/Mpc]	68.09 (68.18) $^{+0.43}_{-0.40}$	69.10 (68.91) $^{+0.66}_{-0.95}$	69.75 (69.19) $^{+0.87}_{-1.2}$	68.5 (68.4) $^{+1.1}_{-0.99}$
$S_8$	0.813 (0.818) $^{+0.010}_{-0.010}$	0.814 (2.483) $^{+0.011}_{-0.011}$	0.812 (0.809) $^{+0.010}_{-0.010}$	0.816 (0.807) $^{+0.011}_{-0.010}$
$H_0$ GT	$4.4\sigma$	$3.2\sigma$	$2.43\sigma$	$3.0\sigma$
$H_0$ IT	$4.12\sigma$	$2.81\sigma$	$2.17\sigma$	$3.08\sigma$

TABLE III: Marginalized posteriors for various model parameters for the  $\Lambda$ CDM, Free-streaming DR, Fluid DR, and Neutrino models, fitting to the dataset: **P18+DESI**. All upper bounds are reported at 95% C.L., for any case where the  $1\sigma$  lower bound is overlapping with our priors. 26

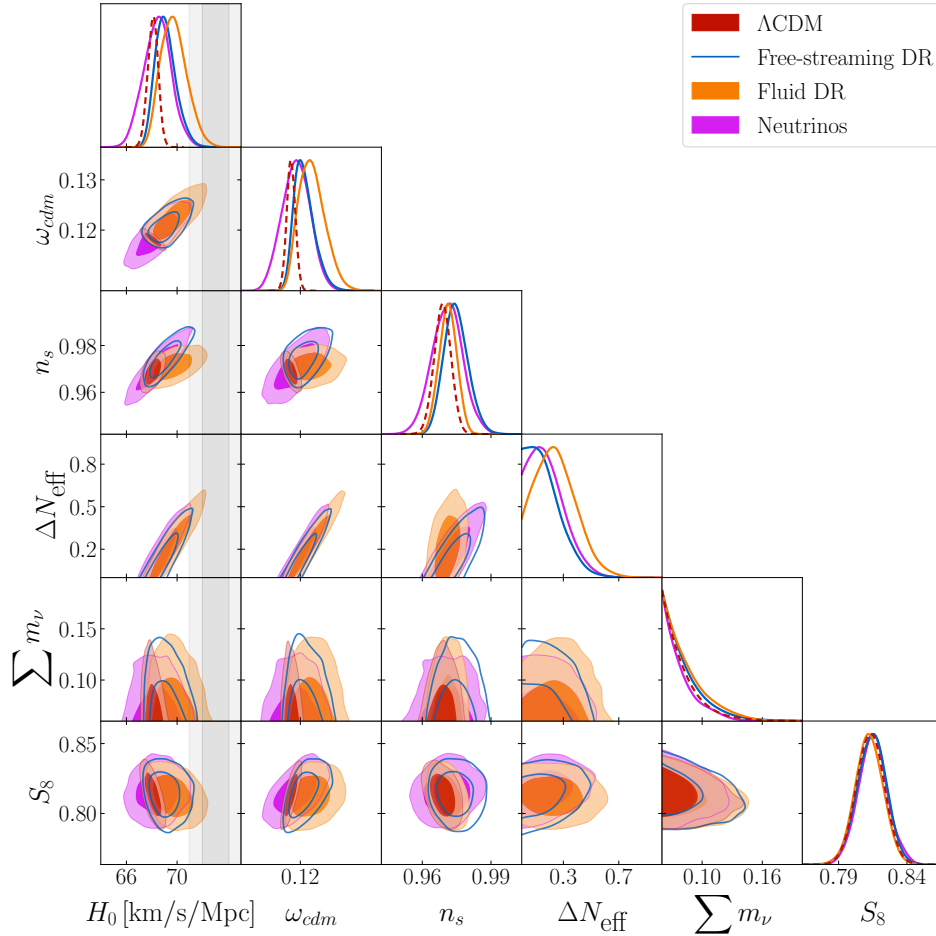


FIG. 4: One and two-dimensional posterior distributions for various model parameters for the  $\Lambda$ CDM, Free-streaming DR, Fluid DR, and Neutrino models, fitting to the dataset: **P18+DESI**. 35

## 2. P18+DESI+Pantheon\_Plus

Parameter	$\Lambda$ CDM	Free-streaming DR	Fluid DR	Neutrinos
$100\omega_b$	2.247 (2.251) $^{+0.013}_{-0.013}$	2.258 (2.246) $^{+0.015}_{-0.016}$	2.265 (2.257) $^{+0.017}_{-0.019}$	2.248 (2.256) $^{+0.019}_{-0.018}$
$\omega_{cdm}$	0.11844 (0.11856) $^{+0.00084}_{-0.00086}$	0.1211 (0.1192) $^{+0.0014}_{-0.0025}$	0.1223 (0.1212) $^{+0.0020}_{-0.0030}$	0.1186 (0.1191) $^{+0.0028}_{-0.0031}$
$\ln 10^{10} A_s$	3.054 (3.061) $^{+0.015}_{-0.016}$	3.061 (3.039) $^{+0.014}_{-0.017}$	3.050 (3.055) $^{+0.015}_{-0.015}$	3.054 (3.052) $^{+0.017}_{-0.018}$
$n_s$	0.9681 (0.9679) $^{+0.0039}_{-0.0036}$	0.9734 (0.9689) $^{+0.0045}_{-0.0058}$	0.9699 (0.9667) $^{+0.0037}_{-0.0039}$	0.9685 (0.9759) $^{+0.0068}_{-0.0069}$
$\tau_{reio}$	0.0602 (0.0636) $^{+0.0074}_{-0.0083}$	0.0606 (0.0537) $^{+0.0071}_{-0.0082}$	0.0605 (0.0619) $^{+0.0072}_{-0.0080}$	0.0601 (0.0608) $^{+0.0071}_{-0.0086}$
$\Delta N_{eff}$	—	$< 0.386$	0.221 (0.128) $^{+0.088}_{-0.18}$	0.06 (0.143) $^{+0.17}_{-0.19}$
$\sum m_\nu$	$< 0.123$	$< 0.137$	$< 0.132$	$< 0.127$
$H_0$ [km/s/Mpc]	67.93 (68.07) $^{+0.44}_{-0.38}$	68.79 (67.99) $^{+0.60}_{-0.89}$	69.35 (68.72) $^{+0.81}_{-1.1}$	68.0 (67.14) $^{+0.97}_{-1.2}$
$S_8$	0.817 (0.822) $^{+0.010}_{-0.010}$	0.818 (0.436) $^{+0.010}_{-0.011}$	0.8161 (0.825) $^{+0.0099}_{-0.0099}$	0.817 (0.821) $^{+0.011}_{-0.011}$
$M_b$	-19.424 (-19.421) $^{+0.013}_{-0.011}$	-19.396 (-19.426) $^{+0.017}_{-0.028}$	-19.381 (-19.4) $^{+0.024}_{-0.033}$	-19.422 (-19.448) $^{+0.030}_{-0.036}$
$H_0$ GT	$4.53\sigma$	$3.53\sigma$	$2.81\sigma$	$3.54\sigma$
$H_0$ IT	$3.93\sigma$	$3.06\sigma$	$2.52\sigma$	$3.22\sigma$

TABLE IV: Marginalized posteriors for various model parameters for the  $\Lambda$ CDM, Free-streaming DR, Fluid DR, and Neutrino models, fitting to the dataset: **P18+DESI+Pantheon\_Plus**. All upper bounds are reported at 95% C.L., for any case where the  $1\sigma$  lower bound is overlapping with our priors.

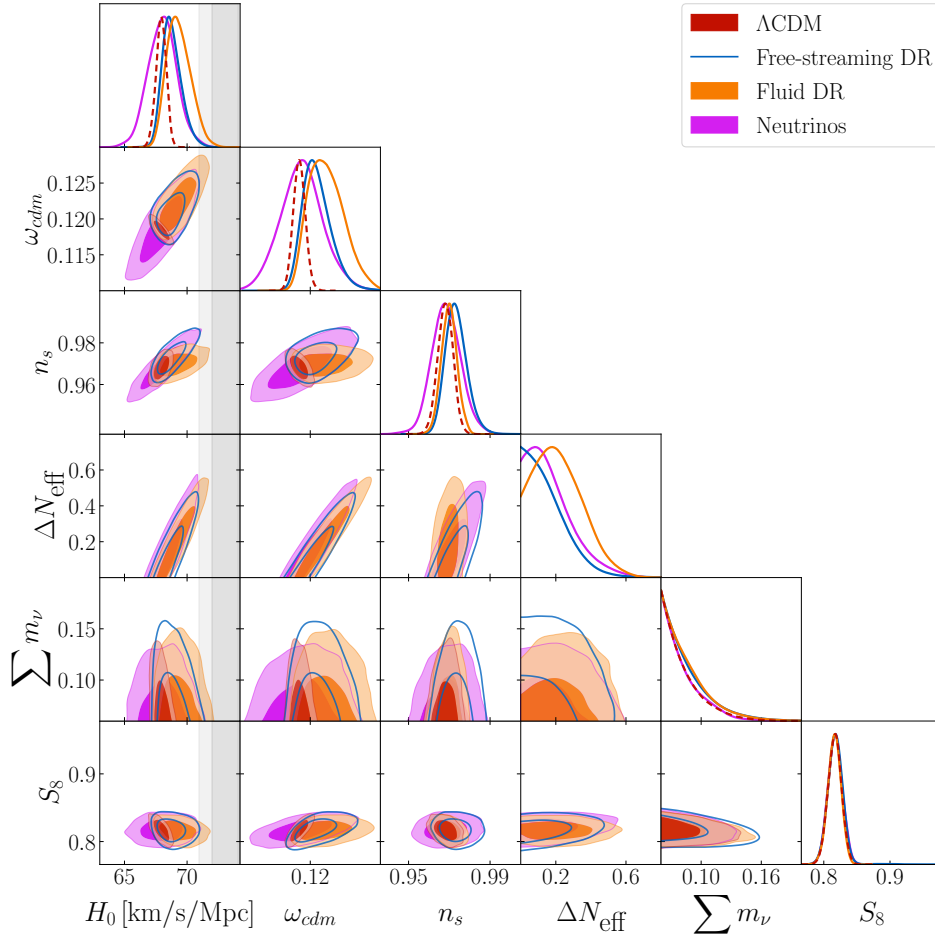


FIG. 5: One and two-dimensional posterior distributions for various model parameters for the  $\Lambda$ CDM, Free-streaming DR, Fluid DR, and Neutrino models, fitting to the dataset: **P18+DESI+Pantheon\_Plus**.

3. P18+DESI+Pantheon\_Plus+H<sub>0</sub>

Parameter	$\Lambda$ CDM	Free-streaming DR	Fluid DR	Neutrinos
$100\omega_b$	2.264 (2.275) $^{+0.013}_{-0.013}$	2.290 (2.289) $^{+0.015}_{-0.015}$	2.304 (2.307) $^{+0.015}_{-0.015}$	2.291 (2.285) $^{+0.014}_{-0.014}$
$\omega_{cdm}$	0.11682 (0.11669) $^{+0.00083}_{-0.00083}$	0.1263 (0.126) $^{+0.0025}_{-0.0025}$	0.1281 (0.1286) $^{+0.0019}_{-0.0016}$	0.1263 (0.1268) $^{+0.0024}_{-0.0024}$
$\ln 10^{10} A_s$	3.061 (3.07) $^{+0.015}_{-0.016}$	3.078 (3.079) $^{+0.015}_{-0.017}$	3.048 (3.042) $^{+0.015}_{-0.016}$	3.078 (3.065) $^{+0.016}_{-0.016}$
$n_s$	0.9723 (0.9732) $^{+0.0037}_{-0.0036}$	0.9871 (0.9867) $^{+0.0049}_{-0.0050}$	0.9746 (0.972) $^{+0.0036}_{-0.0039}$	0.9872 (0.9873) $^{+0.0049}_{-0.0050}$
$\tau_{reio}$	0.0651 (0.0666) $^{+0.0074}_{-0.0085}$	0.0634 (0.0636) $^{+0.0072}_{-0.0086}$	0.0633 (0.0588) $^{+0.0074}_{-0.0077}$	0.0633 (0.0567) $^{+0.0073}_{-0.0084}$
$\Delta N_{\text{eff}}$	—	0.54 (0.52) $^{+0.13}_{-0.13}$	0.592 (0.611) $^{+0.091}_{-0.086}$	0.59 (0.619) $^{+0.12}_{-0.13}$
$\sum m_\nu$	< 0.099	< 0.126	< 0.131	< 0.118
$H_0$ [km/s/Mpc]	68.82 (68.98) $^{+0.37}_{-0.39}$	71.47 (71.39) $^{+0.73}_{-0.76}$	72.13 (72.25) $^{+0.61}_{-0.41}$	71.46 (71.79) $^{+0.73}_{-0.73}$
$S_8$	0.8017 (0.8045) $^{+0.0096}_{-0.010}$	0.822 (0.824) $^{+0.011}_{-0.011}$	0.8095 (0.8086) $^{+0.0097}_{-0.010}$	0.821 (0.819) $^{+0.011}_{-0.011}$
$M_b$	-19.398 (-19.392) $^{+0.011}_{-0.011}$	-19.320 (-19.319) $^{+0.021}_{-0.021}$	-19.301 (-19.295) $^{+0.017}_{-0.011}$	-19.320 (-19.311) $^{+0.021}_{-0.021}$
$H_0$ GT	3.82 $\sigma$	1.23 $\sigma$	0.75 $\sigma$	1.24 $\sigma$
$H_0$ IT	3.8 $\sigma$	1.23 $\sigma$	0.76 $\sigma$	1.24 $\sigma$
$\Delta\chi^2$	—	-19.1	-23.8	-17.5
$\Delta\text{AIC}$	—	-17.1	-21.8	-15.5

TABLE V: Marginalized posteriors for various model parameters for the  $\Lambda$ CDM, Free-streaming DR, Fluid DR, and Neutrino models, fitting to the dataset: **P18+DESI+Pantheon\_Plus+H<sub>0</sub>**. All upper bounds are reported at 95% C.L., for any case where the  $1\sigma$  lower bound is overlapping with our priors.

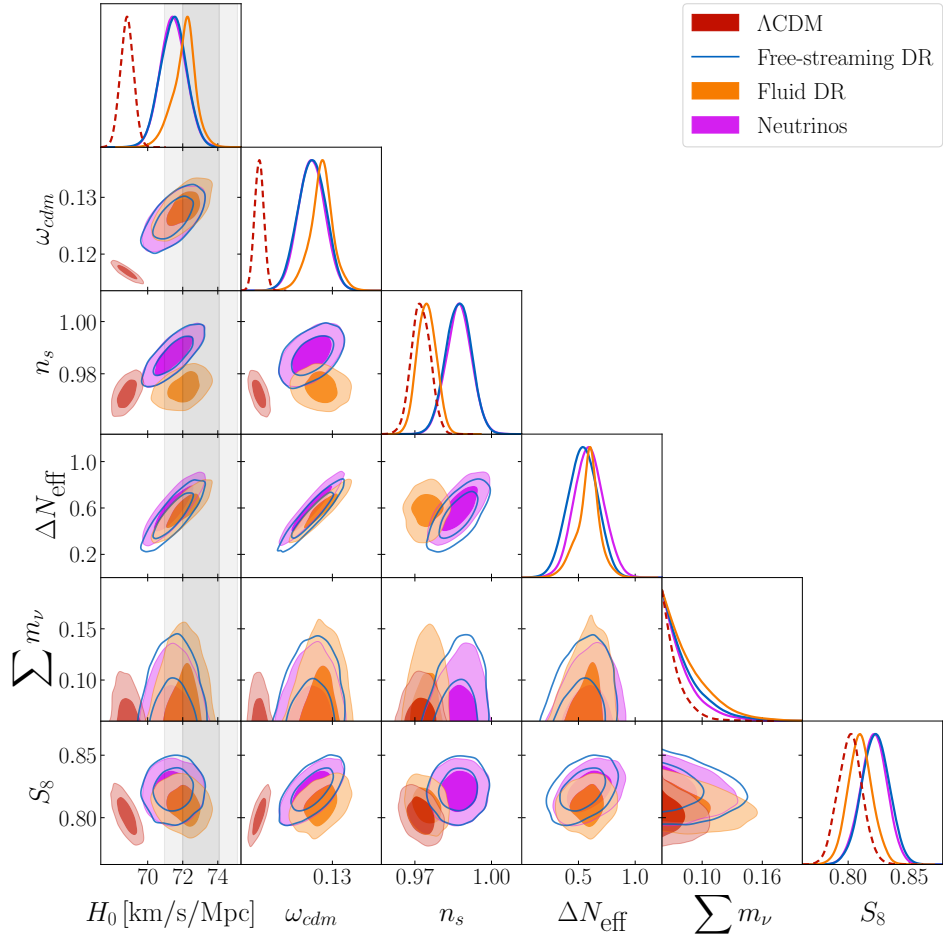


FIG. 6: One and two-dimensional posterior distributions for various model parameters for the  $\Lambda$ CDM, Free-streaming DR, Fluid DR, and Neutrino models, fitting to the dataset: **P18+DESI+Pantheon\_Plus+H<sub>0</sub>**.



4. P18+DESI+Y<sub>He</sub>, D/H

Parameter	$\Lambda$ CDM	Free-streaming DR	Fluid DR	Neutrinos
$100\omega_b$	2.249 (2.24) $^{+0.013}_{-0.013}$	2.254 (2.25) $^{+0.015}_{-0.017}$	2.266 (2.271) $^{+0.016}_{-0.018}$	2.250 (2.23) $^{+0.017}_{-0.018}$
$\omega_{cdm}$	0.11812 (0.11808) $^{+0.00089}_{-0.00087}$	0.1212 (0.1206) $^{+0.0016}_{-0.0021}$	0.1212 (0.1205) $^{+0.0018}_{-0.0026}$	0.1183 (0.1166) $^{+0.0026}_{-0.0026}$
$\ln 10^{10} A_s$	3.055 (3.051) $^{+0.015}_{-0.015}$	3.061 (3.06) $^{+0.015}_{-0.017}$	3.053 (3.061) $^{+0.015}_{-0.016}$	3.055 (3.058) $^{+0.016}_{-0.016}$
$n_s$	0.9689 (0.9676) $^{+0.0036}_{-0.0035}$	0.9743 (0.9754) $^{+0.0050}_{-0.0057}$	0.9707 (0.9723) $^{+0.0039}_{-0.0039}$	0.9693 (0.9629) $^{+0.0064}_{-0.0062}$
$\tau_{reio}$	0.0610 (0.0587) $^{+0.0071}_{-0.0082}$	0.0605 (0.061) $^{+0.0072}_{-0.0083}$	0.0619 (0.0642) $^{+0.0074}_{-0.0083}$	0.0611 (0.0655) $^{+0.0071}_{-0.0083}$
$\Delta N_{eff}$	—	0.179 (0.136) $^{+0.073}_{-0.15}$	0.182 (0.148) $^{+0.061}_{-0.17}$	0.06 (−0.078) $^{+0.16}_{-0.16}$
$\sum m_\nu$	< 0.121	< 0.125	< 0.127	< 0.118
$H_0$ [km/s/Mpc]	68.09 (68.17) $^{+0.42}_{-0.41}$	69.00 (68.86) $^{+0.69}_{-0.93}$	69.30 (69.39) $^{+0.71}_{-1.0}$	68.2 (67.2) $^{+1.0}_{-1.0}$
$S_8$	0.814 (0.814) $^{+0.010}_{-0.010}$	0.817 (1.829) $^{+0.010}_{-0.011}$	0.813 (0.816) $^{+0.011}_{-0.010}$	0.814 (0.822) $^{+0.011}_{-0.011}$
$H_0$ GT	4.42 $\sigma$	3.23 $\sigma$	2.97 $\sigma$	3.37 $\sigma$
$H_0$ IT	3.95 $\sigma$	2.99 $\sigma$	2.66 $\sigma$	3.31 $\sigma$

TABLE VI: Marginalized posteriors for various model parameters for the  $\Lambda$ CDM, Free-streaming DR, Fluid DR, and Neutrino models, fitting to the dataset: **P18+DESI+Y<sub>He</sub>, D/H**. All upper bounds are reported at 95% C.L., for any case where the  $1\sigma$  lower bound is overlapping with our priors.

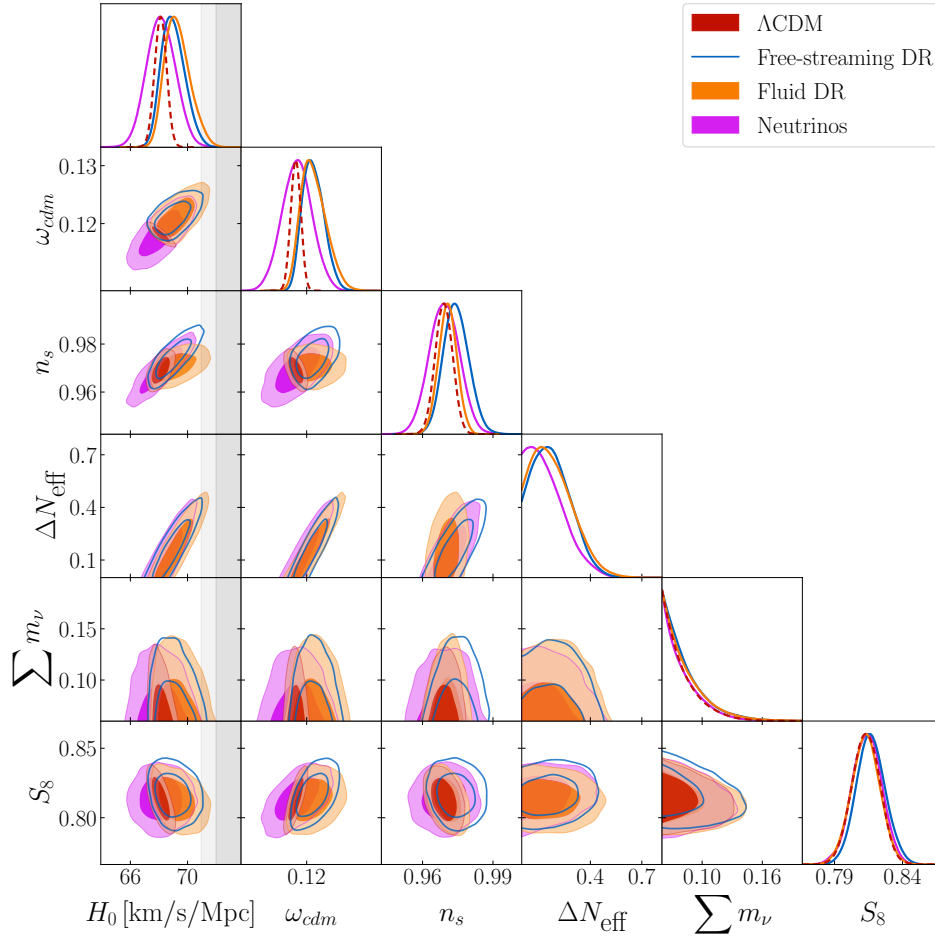


FIG. 7: One and two-dimensional posterior distributions for various model parameters for the  $\Lambda$ CDM, Free-streaming DR, Fluid DR, and Neutrino models, fitting to the dataset: **P18+DESI+Y<sub>He</sub>, D/H**.

5. P18+DESI+Y<sub>He</sub>, D/H+Pantheon\_Plus

Parameter	$\Lambda$ CDM	Free-streaming DR	Fluid DR	Neutrinos
$100\omega_b$	2.247 (2.251) $^{+0.014}_{-0.014}$	2.254 (2.255) $^{+0.014}_{-0.014}$	2.260 (2.242) $^{+0.016}_{-0.016}$	2.249 (2.238) $^{+0.015}_{-0.015}$
$\omega_{cdm}$	0.11845 (0.11833) $^{+0.00084}_{-0.00084}$	0.1203 (0.1196) $^{+0.0013}_{-0.0020}$	0.1213 (0.1187) $^{+0.0016}_{-0.0024}$	0.1191 (0.1183) $^{+0.0015}_{-0.0025}$
$\ln 10^{10} A_s$	3.053 (3.055) $^{+0.014}_{-0.016}$	3.059 (3.061) $^{+0.015}_{-0.017}$	3.052 (3.045) $^{+0.015}_{-0.015}$	3.055 (3.034) $^{+0.015}_{-0.017}$
$n_s$	0.9680 (0.9677) $^{+0.0035}_{-0.0038}$	0.9721 (0.9728) $^{+0.0043}_{-0.0049}$	0.9694 (0.9694) $^{+0.0037}_{-0.0037}$	0.9695 (0.9662) $^{+0.0050}_{-0.0065}$
$\tau_{reio}$	0.0602 (0.0606) $^{+0.0069}_{-0.0081}$	0.0607 (0.0625) $^{+0.0071}_{-0.0084}$	0.0608 (0.058) $^{+0.0071}_{-0.0082}$	0.0599 (0.0519) $^{+0.0070}_{-0.0082}$
$\Delta N_{eff}$	—	$< 0.295$	$< 0.365$	0.087 (−0.007) $^{+0.076}_{-0.15}$
$\sum m_\nu$	$< 0.121$	$< 0.125$	$< 0.131$	$< 0.130$
$H_0$ [km/s/Mpc]	67.92 (68.09) $^{+0.41}_{-0.41}$	68.58 (68.89) $^{+0.55}_{-0.69}$	68.97 (68.0) $^{+0.65}_{-0.93}$	68.13 (67.53) $^{+0.68}_{-0.96}$
$S_8$	0.817 (0.817) $^{+0.010}_{-0.0098}$	0.819 (0.816) $^{+0.010}_{-0.011}$	0.816 (0.819) $^{+0.010}_{-0.010}$	0.817 (0.818) $^{+0.010}_{-0.0097}$
$M_b$	−19.424 (−19.421) $^{+0.012}_{-0.012}$	−19.404 (−19.393) $^{+0.016}_{-0.021}$	−19.392 (−19.423) $^{+0.020}_{-0.028}$	−19.418 (−19.436) $^{+0.020}_{-0.029}$
$H_0$ GT	4.58 $\sigma$	3.8 $\sigma$	3.31 $\sigma$	3.96 $\sigma$
$H_0$ IT	3.79 $\sigma$	3.42 $\sigma$	2.93 $\sigma$	3.68 $\sigma$

TABLE VII: Marginalized posteriors for various model parameters for the  $\Lambda$ CDM, Free-streaming DR, Fluid DR, and Neutrino models, fitting to the dataset: **P18+DESI+Y<sub>He</sub>, D/H+Pantheon\_Plus**. All upper bounds are reported at 95% C.L., for any case where the  $1\sigma$  lower bound is overlapping with our priors.

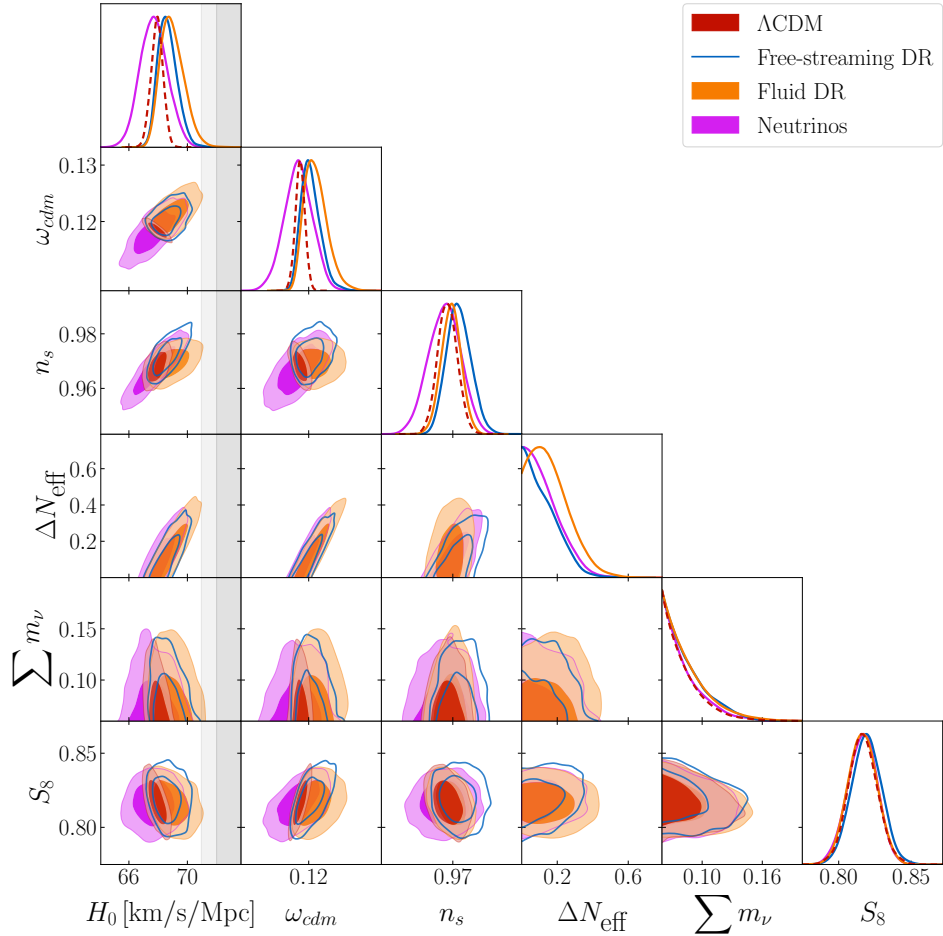


FIG. 8: One and two-dimensional posterior distributions for various model parameters for the  $\Lambda$ CDM, Free-streaming DR, Fluid DR, and Neutrino models, fitting to the dataset: **P18+DESI+Y<sub>He</sub>, D/H+Pantheon\_Plus**.

6. P18+DESI+Y<sub>He</sub>, D/H+Pantheon\_Plus+H<sub>0</sub>

Parameter	$\Lambda$ CDM	Free-streaming DR	Fluid DR	Neutrinos 4
$100\omega_b$	2.264 (2.273) $^{+0.013}_{-0.013}$	2.285 (2.28) $^{+0.014}_{-0.014}$	2.295 (2.296) $^{+0.015}_{-0.015}$	2.287 (2.284) $^{+0.015}_{-0.014}$
$\omega_{cdm}$	0.11685 (0.11643) $^{+0.00081}_{-0.00081}$	0.1248 (0.1238) $^{+0.0019}_{-0.0019}$	0.1260 (0.1256) $^{+0.0024}_{-0.0024}$	0.1244 (0.1229) $^{+0.0023}_{-0.0023}$
$\ln 10^{10} A_s$	3.060 (3.068) $^{+0.015}_{-0.017}$	3.076 (3.057) $^{+0.015}_{-0.017}$	3.051 (3.042) $^{+0.015}_{-0.017}$	3.075 (3.063) $^{+0.016}_{-0.017}$
$n_s$	0.9723 (0.9721) $^{+0.0035}_{-0.0036}$	0.9849 (0.9825) $^{+0.0048}_{-0.0047}$	0.9742 (0.9747) $^{+0.0037}_{-0.0037}$	0.9844 (0.9832) $^{+0.0050}_{-0.0049}$
$\tau_{reio}$	0.0647 (0.0677) $^{+0.0073}_{-0.0084}$	0.0635 (0.0557) $^{+0.0071}_{-0.0087}$	0.0636 (0.0604) $^{+0.0070}_{-0.0087}$	0.0639 (0.0615) $^{+0.0074}_{-0.0084}$
$\Delta N_{eff}$	—	0.45 (0.38) $^{+0.10}_{-0.10}$	0.48 (0.48) $^{+0.11}_{-0.11}$	0.49 (0.431) $^{+0.12}_{-0.12}$
$\sum m_\nu$	< 0.099	< 0.120	< 0.128	< 0.115 13
$H_0$ [km/s/Mpc]	68.81 (69.12) $^{+0.37}_{-0.37}$	71.02 (70.59) $^{+0.69}_{-0.67}$	71.46 (71.78) $^{+0.74}_{-0.72}$	70.95 (71.06) $^{+0.70}_{-0.70}$
$S_8$	0.8015 (0.8005) $^{+0.0098}_{-0.0098}$	0.817 (2.701) $^{+0.010}_{-0.010}$	0.8090 (0.8007) $^{+0.0099}_{-0.010}$	0.817 (0.807) $^{+0.011}_{-0.011}$
$M_b$	-19.398 (-19.387) $^{+0.011}_{-0.011}$	-19.332 (-19.341) $^{+0.019}_{-0.020}$	-19.321 (-19.31) $^{+0.021}_{-0.021}$	-19.335 (-19.332) $^{+0.020}_{-0.020}$
$H_0$ GT	3.83 $\sigma$	1.62 $\sigma$	1.24 $\sigma$	1.67 $\sigma$
$H_0$ IT	3.84 $\sigma$	1.62 $\sigma$	1.24 $\sigma$	1.67 $\sigma$
$\Delta\chi^2$	—	-12.7	-17.7	-10.5
$\Delta AIC$	—	-10.7	-15.7	-8.5

TABLE VIII: Marginalized posteriors for various model parameters for the  $\Lambda$ CDM, Free-streaming DR, Fluid DR, and Neutrino models, fitting to the dataset: **P18+DESI+Y<sub>He</sub>, D/H+Pantheon\_Plus+H<sub>0</sub>**. All upper bounds are reported at 95% C.L., for any case where the  $1\sigma$  lower bound is overlapping with our priors.

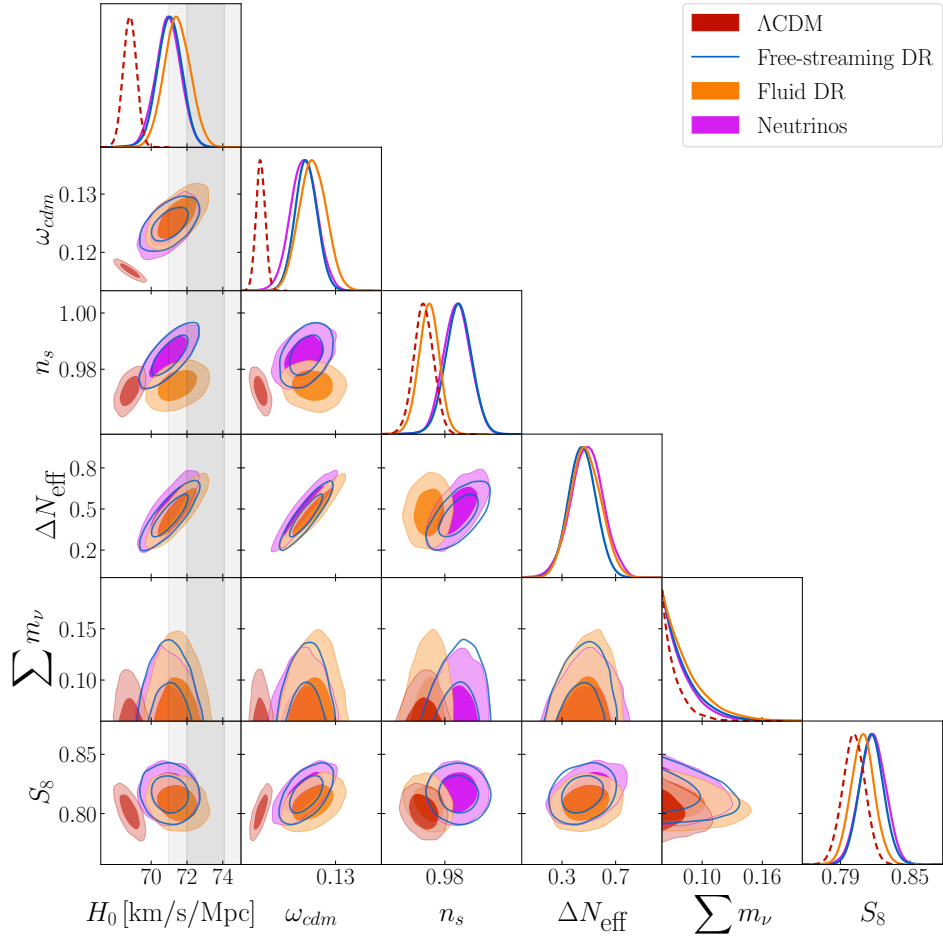


FIG. 9: One and two-dimensional posterior distributions for various model parameters for the  $\Lambda$ CDM, Free-streaming DR, Fluid DR, and Neutrino models, fitting to the dataset: **P18+DESI+Y<sub>He</sub>, D/H+Pantheon\_Plus+H<sub>0</sub>**.

## 7. P18+SDSS+6dFGS+Pantheon\_Plus

Parameter	$\Lambda$ CDM	Free-streaming DR	Fluid DR	Neutrinos
$100\omega_b$	2.238 (2.253) $^{+0.013}_{-0.013}$	2.246 (2.248) $^{+0.015}_{-0.015}$	2.251 (2.252) $^{+0.016}_{-0.016}$	2.232 (2.23) $^{+0.018}_{-0.018}$
$\omega_{cdm}$	0.11964 (0.11931) $^{+0.00090}_{-0.00089}$	0.1217 (0.1202) $^{+0.0012}_{-0.0012}$	0.1223 (0.1204) $^{+0.0015}_{-0.0025}$	0.1183 (0.1177) $^{+0.0028}_{-0.0031}$
$\ln 10^{10} A_s$	3.049 (3.053) $^{+0.013}_{-0.015}$	3.055 (3.049) $^{+0.014}_{-0.016}$	3.048 (3.048) $^{+0.014}_{-0.016}$	3.045 (3.051) $^{+0.016}_{-0.016}$
$n_s$	0.9652 (0.9653) $^{+0.0036}_{-0.0037}$	0.9691 (0.9698) $^{+0.0039}_{-0.0053}$	0.9666 (0.9656) $^{+0.0038}_{-0.0038}$	0.9621 (0.9615) $^{+0.0069}_{-0.0068}$
$\tau_{reio}$	0.0572 (0.0578) $^{+0.0067}_{-0.0075}$	0.0570 (0.0563) $^{+0.0069}_{-0.0078}$	0.0577 (0.056) $^{+0.0068}_{-0.0080}$	0.0568 (0.0597) $^{+0.0067}_{-0.0075}$
$\Delta N_{eff}$	—	$< 0.312$	$< 0.285$	$-0.04 (-0.061)^{+0.18}_{-0.18}$
$\sum m_\nu$	$< 0.152$	$< 0.174$	$< 0.169$	$< 0.146$
$H_0$ [km/s/Mpc]	67.27 (67.78) $^{+0.43}_{-0.43}$	67.84 (67.79) $^{+0.58}_{-0.75}$	68.25 (67.83) $^{+0.69}_{-0.98}$	66.8 (66.9) $^{+1.1}_{-1.1}$
$S_8$	0.827 (0.826) $^{+0.011}_{-0.011}$	0.826 (5.249) $^{+0.012}_{-0.012}$	0.826 (0.828) $^{+0.011}_{-0.011}$	0.826 (0.826) $^{+0.011}_{-0.011}$
$M_b$	-19.443 (-19.43) $^{+0.013}_{-0.013}$	-19.421 (-19.426) $^{+0.015}_{-0.026}$	-19.412 (-19.427) $^{+0.021}_{-0.030}$	-19.458 (-19.455) $^{+0.034}_{-0.035}$
$H_0$ GT	$5.12\sigma$	$4.37\sigma$	$3.83\sigma$	$4.19\sigma$
$H_0$ IT	$5.11\sigma$	$3.53\sigma$	$3.35\sigma$	$4.24\sigma$

TABLE IX: Marginalized posteriors for various model parameters for the  $\Lambda$ CDM, Free-streaming DR, Fluid DR, and Neutrino models, fitting to the dataset: **P18+SDSS+6dFGS+Pantheon\_Plus**. All upper bounds are reported at 95% C.L., for any case where the  $1\sigma$  lower bound is overlapping with our priors.

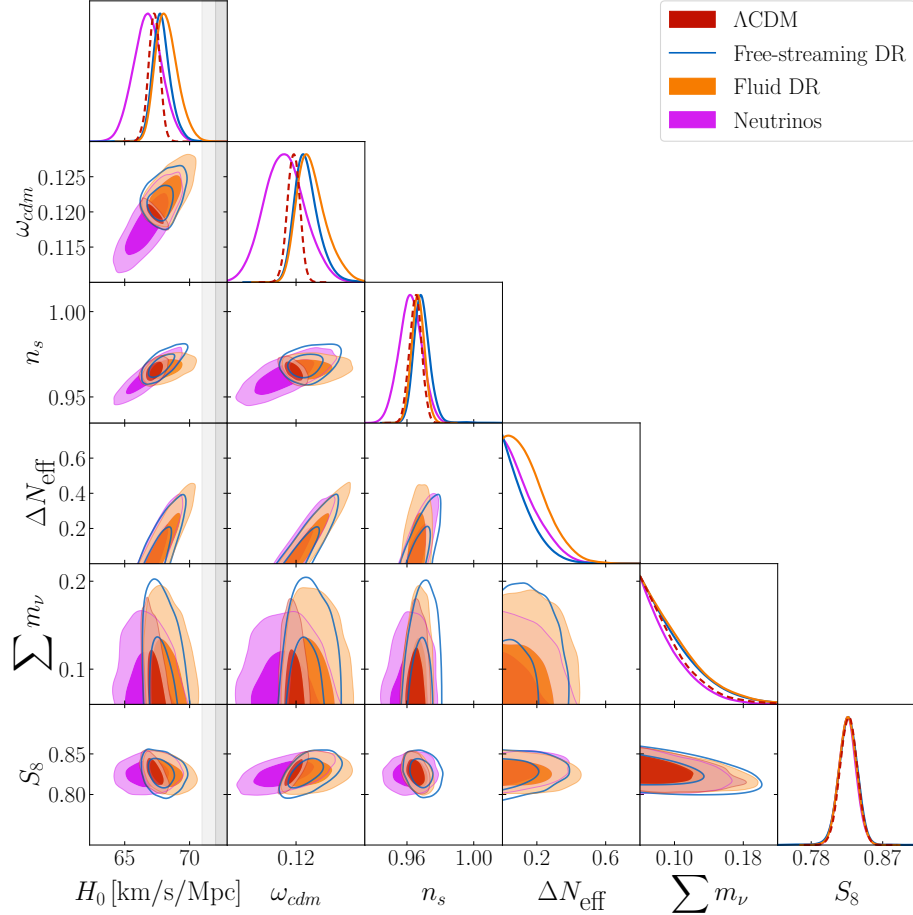


FIG. 10: One and two-dimensional posterior distributions for various model parameters for the  $\Lambda$ CDM, Free-streaming DR, Fluid DR, and Neutrino models, fitting to the dataset: **P18+SDSS+6dFGS+Pantheon\_Plus**.



## 8. Fluid Dark Radiation Produced After BBN 122

Parameter	P18+SDSS+6dFGS+Pantheon_Plus	P18+DESI+Pantheon_Plus	P18+DESI+Pantheon_Plus+H <sub>0</sub>
$100\omega_b$	2.251 (2.241) $^{+0.015}_{-0.017}$	2.266 (2.263) $^{+0.015}_{-0.019}$	2.299 (2.305) $^{+0.015}_{-0.015}$
$\omega_{cdm}$	0.1228 (0.1219) $^{+0.0018}_{-0.0028}$	0.1229 (0.1254) $^{+0.0023}_{-0.0034}$	0.1291 (0.1303) $^{+0.0028}_{-0.0028}$
$\ln 10^{10} A_s$	3.047 (3.049) $^{+0.015}_{-0.015}$	3.049 (3.041) $^{+0.015}_{-0.015}$	3.045 (3.053) $^{+0.016}_{-0.016}$
$n_s$ 142	0.9658 (0.9652) $^{+0.0038}_{-0.0037}$	0.9689 (0.9666) $^{+0.0037}_{-0.0037}$	0.9716 (0.9759) $^{+0.0035}_{-0.0035}$
$\tau_{reio}$	0.0575 (0.057) $^{+0.0069}_{-0.0075}$	0.0607 (0.057) $^{+0.0071}_{-0.0081}$	0.0627 (0.0679) $^{+0.0073}_{-0.0083}$
$\Delta N_{eff}$	< 0.433	0.26 (0.34) $^{+0.11}_{-0.21}$ 117	0.65 (0.73) $^{+0.13}_{-0.14}$
$\sum m_\nu$	< 0.166	< 0.137	< 0.149
$H_0$ [km/s/Mpc]	68.39 (67.94) $^{+0.71}_{-1.1}$	69.56 (69.82) $^{+0.85}_{-1.2}$	72.25 (73.0) $^{+0.79}_{-0.79}$
$S_8$	0.826 (0.834) $^{+0.011}_{-0.011}$	0.815 (0.825) $^{+0.010}_{-0.011}$	0.809 (0.812) $^{+0.011}_{-0.011}$
$M_b$	-19.408 (-19.42) $^{+0.022}_{-0.033}$	-19.374 (-19.365) $^{+0.026}_{-0.037}$	-19.298 (-19.276) $^{+0.024}_{-0.021}$
$H_0$ GT	3.69 $\sigma$	2.59 $\sigma$ 127	0.6 $\sigma$
$H_0$ IT	3.02 $\sigma$	2.28 $\sigma$ 128	0.6 $\sigma$
$\Delta\chi^2$	$\sim 0$	-0.4	-24.7
$\Delta AIC$	+2.0	+1.6	-22.7

TABLE X: Marginalized posteriors for various model parameters for the Fluid DR model where the DR is produced after BBN. The fit is shown for the datasets **P18+SDSS+6dFGS+Pantheon\_Plus**, **P18+DESI+Pantheon\_Plus**, and **P18+DESI+Pantheon\_Plus+H<sub>0</sub>**. All upper bounds are reported at 95% C.L., for any case where the  $1\sigma$  lower bound is overlapping with our priors.

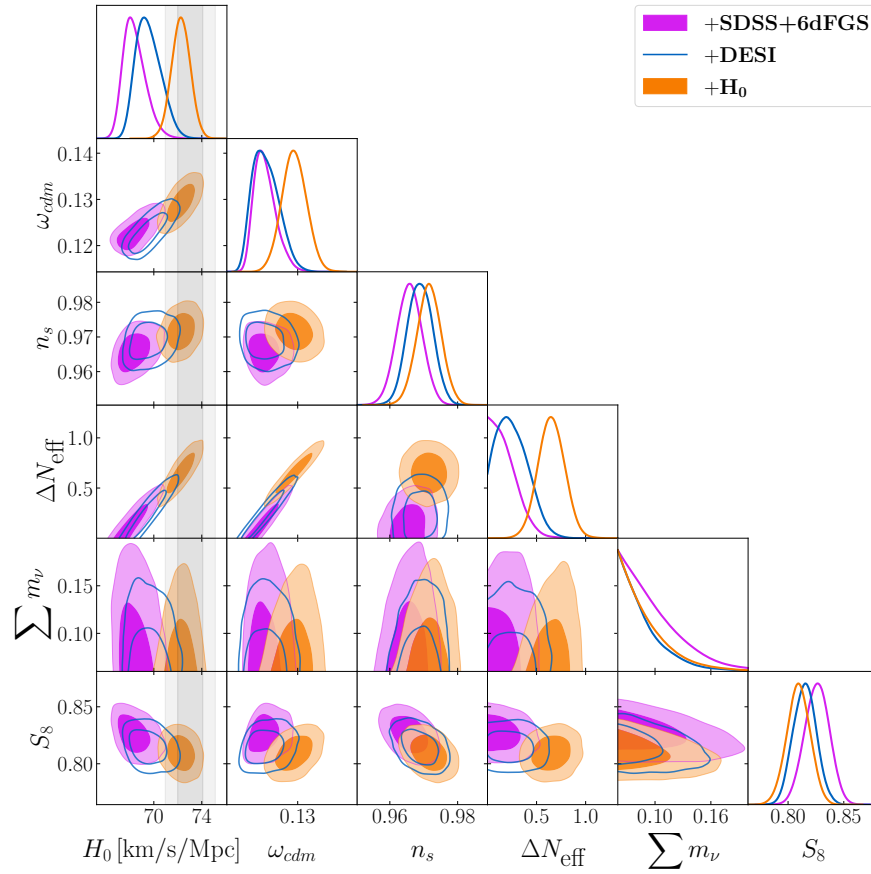


FIG. 11: One and two-dimensional posterior distributions for various model parameters for the Fluid DR model where the DR is produced after BBN. The fit is shown for the datasets **P18+SDSS+6dFGS+Pantheon\_Plus**, **P18+DESI+Pantheon\_Plus**, and **P18+DESI+Pantheon\_Plus+H<sub>0</sub>**.

## 9. Free-streaming Dark Radiation Produced After BBN 33

Parameter	P18+SDSS+6dFGS+Pantheon_Plus	P18+DESI+Pantheon_Plus	P18+DESI+Pantheon_Plus+H <sub>0</sub>
$100\omega_b$	2.245 (2.24) $^{+0.015}_{-0.014}$	2.257 (2.254) $^{+0.015}_{-0.016}$	2.288 (2.278) $^{+0.014}_{-0.014}$
$\omega_{cdm}$	0.1219 (0.1218) $^{+0.0014}_{-0.0024}$	0.1214 (0.1193) $^{+0.0016}_{-0.0027}$	0.1278 (0.1287) $^{+0.0026}_{-0.0026}$
$\ln 10^{10} A_s$	3.054 (3.041) $^{+0.015}_{-0.016}$	3.060 (3.059) $^{+0.014}_{-0.017}$	3.077 (3.071) $^{+0.014}_{-0.017}$
$n_s$ 4	0.9688 (0.9676) $^{+0.0043}_{-0.0050}$	0.9731 (0.9732) $^{+0.0045}_{-0.0055}$	0.9864 (0.987) $^{+0.0044}_{-0.0047}$
$\tau_{reio}$	0.0568 (0.0493) $^{+0.0068}_{-0.0079}$	0.0602 (0.0623) $^{+0.0071}_{-0.0081}$	0.0622 (0.0584) $^{+0.0069}_{-0.0084}$
$\Delta N_{\text{eff}}$	< 0.353	< 0.435	0.63 (0.65) $^{+0.14}_{-0.14}$
$\sum m_\nu$	< 0.161	< 0.129	< 0.137
$H_0$ [km/s/Mpc]	68.03 (68.17) $^{+0.57}_{-0.84}$	68.94 (68.41) $^{+0.63}_{-0.99}$	71.82 (71.65) $^{+0.78}_{-0.77}$
$S_8$	0.830 (0.826) $^{+0.011}_{-0.011}$	0.821 (0.822) $^{+0.011}_{-0.011}$	0.823 (0.83) $^{+0.011}_{-0.011}$
$M_b$	-19.419 (-19.414) $^{+0.017}_{-0.026}$	-19.393 (-19.41) $^{+0.019}_{-0.030}$	-19.310 (-19.311) $^{+0.022}_{-0.022}$
$H_0$ GT	4.22 $\sigma$	3.37 $\sigma$ 41	0.94 $\sigma$
$H_0$ IT	3.62 $\sigma$	2.84 $\sigma$ 42	0.94 $\sigma$
$\Delta\chi^2$	$\sim 0$	+0.4	-20.5
$\Delta\text{AIC}$	+2.0	+2.4	-18.5

TABLE XI: Marginalized posteriors for various model parameters for the Fluid DR model where the DR is produced after BBN. The fit is shown for the datasets **P18+DESI+Pantheon.Plus** and **P18+DESI+Pantheon.Plus+H<sub>0</sub>**. All upper bounds are reported at 95% C.L., for any case where the  $1\sigma$  lower bound is overlapping with our priors.

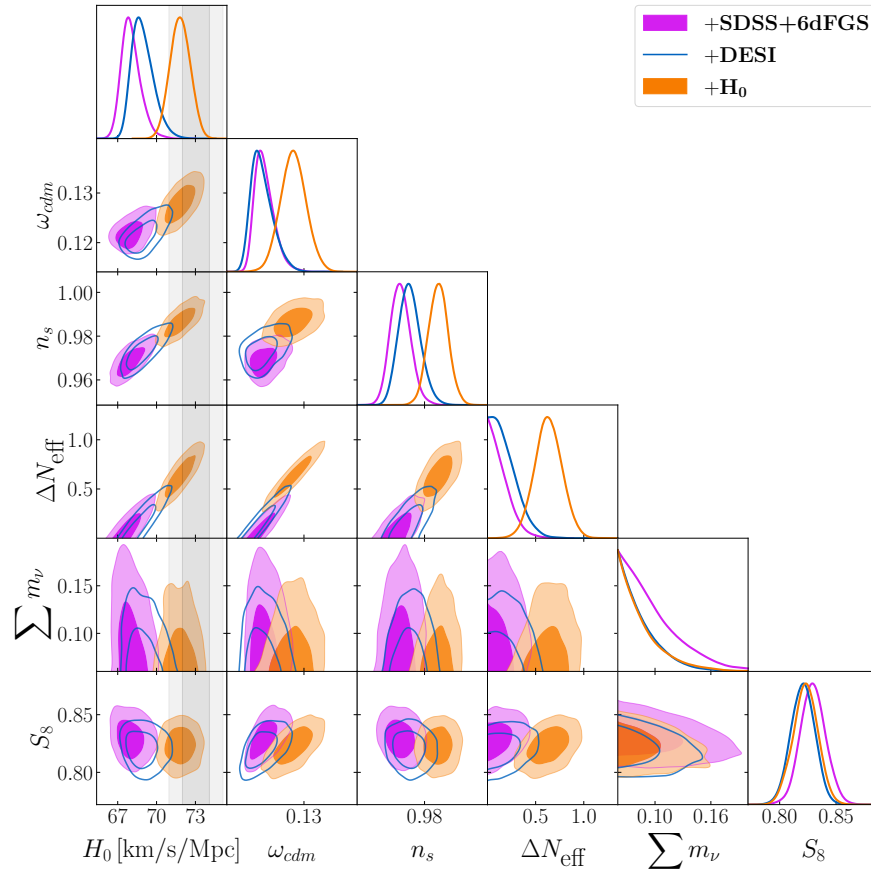


FIG. 12: One and two-dimensional posterior distributions for various model parameters for the free-streaming DR model where the DR is produced after BBN. The fit is shown for the datasets **P18+DESI+Pantheon.Plus** and **P18+DESI+Pantheon.Plus+H<sub>0</sub>**.